



**HAL**  
open science

## A Comparative Analysis of Satellite-Derived CO Retrievals During the 2020 Wildfires in North America

Heba S Marey, James R Drummond, Dylan B A Jones, Helen Worden, Cathy Clerbaux, Tobias Borsdorff, John Gille

► **To cite this version:**

Heba S Marey, James R Drummond, Dylan B A Jones, Helen Worden, Cathy Clerbaux, et al.. A Comparative Analysis of Satellite-Derived CO Retrievals During the 2020 Wildfires in North America. *Journal of Geophysical Research: Atmospheres*, 2024, 129 (22), pp.e2023JD039876. 10.1029/2023jd039876 . insu-04804718

**HAL Id: insu-04804718**

**<https://insu.hal.science/insu-04804718v1>**

Submitted on 26 Nov 2024

**HAL** is a multi-disciplinary open access archive for the deposit and dissemination of scientific research documents, whether they are published or not. The documents may come from teaching and research institutions in France or abroad, or from public or private research centers.

L'archive ouverte pluridisciplinaire **HAL**, est destinée au dépôt et à la diffusion de documents scientifiques de niveau recherche, publiés ou non, émanant des établissements d'enseignement et de recherche français ou étrangers, des laboratoires publics ou privés.



Distributed under a Creative Commons Attribution - NonCommercial - NoDerivatives 4.0 International License

# JGR Atmospheres

## RESEARCH ARTICLE

10.1029/2023JD039876

### Key Points:

- All the three CO satellite instruments (Measurements of Pollution in the Troposphere, Infrared Atmospheric Sounding Interferometer (IASI), and Tropospheric Monitoring Instrument (TROPOMI)) show excellent agreement under typical atmospheric CO conditions
- The CO data from the three sensors indicated large discrepancies in regions
- The very high IASI and TROPOMI CO observations over the PNW coincide with the high TROPOMI aerosol index values

### Supporting Information:

Supporting Information may be found in the online version of this article.

### Correspondence to:

H. S. Marey,  
hmarey@atmosp.physics.utoronto.ca

### Citation:

Marey, H. S., Drummond, J. R., Jones, D. B. A., Worden, H., Clerbaux, C., Borsdorff, T., & Gille, J. (2024). A comparative analysis of satellite-derived CO retrievals during the 2020 wildfires in North America. *Journal of Geophysical Research: Atmospheres*, 129, e2023JD039876. <https://doi.org/10.1029/2023JD039876>

Received 4 OCT 2023  
Accepted 31 OCT 2024






### Author Contributions:

**Conceptualization:** Heba S. Marey, James R. Drummond  
**Formal analysis:** Heba S. Marey, James R. Drummond  
**Funding acquisition:** James R. Drummond  
**Investigation:** Heba S. Marey, James R. Drummond, Dylan B. A. Jones  
**Methodology:** Heba S. Marey  
**Project administration:** James R. Drummond, Dylan B. A. Jones

© 2024. The Author(s).

This is an open access article under the terms of the [Creative Commons Attribution-NonCommercial-NoDerivs License](#), which permits use and distribution in any medium, provided the original work is properly cited, the use is non-commercial and no modifications or adaptations are made.

# A Comparative Analysis of Satellite-Derived CO Retrievals During the 2020 Wildfires in North America

Heba S. Marey<sup>1</sup> , James R. Drummond<sup>1</sup>, Dylan B. A. Jones<sup>1</sup> , Helen Worden<sup>2</sup> ,  
Cathy Clerbaux<sup>3</sup> , Tobias Borsdorff<sup>4</sup> , and John Gille<sup>2</sup>

<sup>1</sup>Department of Physics, University of Toronto, Toronto, ON, Canada, <sup>2</sup>National Center for Atmospheric Research, Boulder, CO, USA, <sup>3</sup>LATMOS/IPSL, Sorbonne Université, UVSQ, CNRS, Paris, France, <sup>4</sup>Earth Science Group, SRON Netherlands Institute for Space Research, Leiden, The Netherlands

**Abstract** In September 2020, the Western United States experienced anomalously severe wildfires that resulted in carbon monoxide (CO) emissions almost three times the 2001–2019 average. In this study, we investigate the influence of wildfires on atmospheric carbon monoxide (CO) variability through a comparative analysis of observations from the Measurements of Pollution in the Troposphere (MOPITT), the Infrared Atmospheric Sounding Interferometer (IASI), and the Tropospheric Monitoring Instrument (TROPOMI). Our focus is on the North American domain, aiming to understand the differences among these products. In general, all instruments show excellent agreement under typical atmospheric CO conditions. However, notable discrepancies were observed in the CO data from the three sensors, particularly in regions with elevated CO total column (TC) values. IASI and TROPOMI consistently showed higher CO values over the western U.S. compared to MOPITT. During the fire episodes, we found that the IASI retrievals suggested higher CO abundances near the surface than the MOPITT thermal infrared retrievals that are probably the result of the differences in the covariance matrices used in IASI and MOPITT retrievals. We also found that the high IASI and TROPOMI CO observations over the western U.S. coincided with high values of the TROPOMI aerosol index (AI), suggesting the presence of absorbing aerosols. The analysis exhibited better agreement between TROPOMI and MOPITT CO TC when the AI values were low. Our results suggest that appropriate quality filtering should be employed when analyzing pollution events with these data. In particular, utilizing the AI for quality filtering may be useful when analyzing extreme pollution events with these satellite products.

**Plain Language Summary** In September 2020, wildfires in the Western U.S. caused large smoke plumes that spread across the continent, significantly increasing atmospheric carbon monoxide (CO) levels. Using data from the MOPITT, IASI, and TROPOMI satellite sensors, this study found strong CO enhancements from the fires. The sensors showed good agreement under moderate CO conditions but diverged in areas of high CO and heavy aerosol loads, suggesting aerosol interference in CO retrievals. TROPOMI's UV Aerosol Index (AI) and CALIPSO data were used to evaluate aerosol impacts, emphasizing the need for quality filtering when analyzing CO during intense pollution events.

## 1. Introduction

Wildfires significantly impact atmospheric composition by emitting both long and short-lived trace gases and aerosols into the atmosphere (Voulgarakis et al., 2015), which can have adverse effects on air quality. Air quality is crucial for human health and quality of life, and the influence of fires on air quality is becoming increasingly concerning (Finlay et al., 2012). Notably, wildfires can lead to significant increases in the concentrations of carbon monoxide (CO), ozone (O<sub>3</sub>), nitrogen oxides (NO<sub>x</sub>), and fine particulate matter (PM<sub>2.5</sub>), all of which can adversely affect air quality (Phuleria et al., 2011). Exposure to wildfire smoke emissions is associated with a range of health impacts for communities near the wildfires and those downwind due to long-range transport (Bates et al., 1995; Youssouf et al., 2014). For instance, wildfires in the Pacific Northwest (PNW) region have been observed to significantly impact tropospheric composition in the North Atlantic Basin (Lapina et al., 2006), indicating that these fires play a substantial role in shaping tropospheric composition throughout much of the Northern Hemisphere. Moreover, the release of greenhouse gases such as carbon dioxide (CO<sub>2</sub>) from forest fires contributes to global warming and climate change, thereby impacting weather patterns and ecosystems (McClure & Jaffe, 2018).

**Resources:** James R. Drummond, Dylan B. A. Jones, Helen Worden, Cathy Clerbaux, Tobias Borsdorff, John Gille  
**Software:** Heba S. Marey  
**Supervision:** James R. Drummond, Dylan B. A. Jones, Helen Worden  
**Validation:** Heba S. Marey  
**Visualization:** Heba S. Marey, Cathy Clerbaux  
**Writing – original draft:** Heba S. Marey  
**Writing – review & editing:** James R. Drummond, Dylan B. A. Jones, Helen Worden, Cathy Clerbaux, Tobias Borsdorff, John Gille

The frequency and size of wildfires in the United States, particularly in the Western region, have been increasing over the past decades and are expected to continue rising due to global climate change (Scholze et al., 2006; Westerling, A. L., 2016; Schneising et al., 2020). Satellite observations of the burned area from the Moderate Resolution Imaging Spectrometer (MODIS) and satellite-based estimates of fire CO<sub>2</sub> emissions from the global fire emissions database (GFED4s) indicate hotspots over the PNW (Pacific Northwest) in August and September. The inter-annual variability of fires in this region is characterized by increased fire activity in certain years, notably in 1988, 2006, 2012, 2017, 2018, and 2020, with the highest level recorded in 2020 (Xie et al., 2022). In particular, the year 2020 experienced an anomalously large wildfire season in the Western U.S. Numerous fires in California, Colorado, Washington, and Oregon resulted in the burning of over 10 million acres. It was reported that those fires resulted in extensive damage, including fatalities and property loss (Abatzoglou et., 2021; Higuera & Abatzoglou, 2021). Albores et al. (2023) highlighted the remarkable significance of the 2020 U.S. wildfire season, noting that carbon monoxide (CO) emissions surpassed three times the average annual emissions observed between 2001 and 2019. Additionally, their study showed that Western U.S. fires contributed to more than half of the U.S. wildfire emissions in 2020.

During the latter half of the summer of 2020, the Pacific Northwest (PNW) experienced above-normal temperatures and below-normal precipitation (Reilly et al., 2022). The region's vegetation primarily consists of dense conifer forests and brush, with the PNW containing the world's largest seasonal temperate rainforests along the Oregon Cascades (DellaSala, 2014). By early September, an exceptionally warm environment and severe drought conditions led to vegetation becoming highly dry and combustible. These circumstances, coupled with strong, unusual easterly and north-easterly winds, played a significant role in the rapid spread of fires (Abatzoglou et al., 2021; Mass et al., 2021; Varga et al., 2022).

Additionally, the atmospheric transport of biomass emissions in the PNW is impacted by the complex topography, which consists of a basin with high mountains along the coastal region (Nakata et al., 2022). High-resolution numerical simulations suggested the importance of high-amplitude mountain waves that produce strong easterly winds over and to the west of the crest of the Oregon Cascades (Mass et al., 2021). Evers et al. (2022) found that burn severity was linked to vegetation type and the elevation and slope of the topography of the region, with slope having the greatest effect. The steep slopes enhanced the fire severity as trees have more wind exposure, convective heating, and higher fire ventilation and turbulence. As a result of stronger winds, the fire activity is amplified at relatively higher elevations (Evers et al., 2022).

Despite efforts made in recent decades to mitigate human-made pollution, the air quality in fire-prone regions of North America has deteriorated due to the increasing frequency of wildfires (Buchholz et al., 2022; McClure & Jaffe, 2018). Thus, understanding the impact of local and transported pollution on air quality is critical for the mitigation of future adverse health effects. However, the quantification of wildfire emissions and impacts has many challenges as fires often ignite sporadically in remote regions that are hard to access from the ground. Aircraft can sample wildfire plumes but are not able to sample close to the fire or for the entire fire season. On the other hand, satellite instruments can measure directly over plumes with consistent, frequent, and extensive data coverage at regional and global scales, but with a relatively large footprint.

One approach for estimating fire carbon emissions (Liu et al., 2017; Yin et al., 2016) involves utilizing satellite observations of atmospheric CO, which is commonly emitted alongside gases like CO<sub>2</sub> during incomplete combustion in wildfires, and which serves as a vital tracer for fire activity (Andreae & Merlet, 2001). Analyzing CO distributions resulting from wildfire emissions provides insights into related atmospheric species, such as tropospheric ozone and aerosols. Furthermore, given its relatively long lifetime in the atmosphere, CO acts as an indicator for long-range pollution transport (Andreae & Merlet, 2001).

A critical aspect of evaluating fire carbon emissions involves comparing satellite observations from several instruments such as: MOPITT (Measurements of Pollution in the Troposphere), TROPOMI (TROPOspheric Monitoring Instrument), and IASI (Infrared Atmospheric Sounding Interferometer). These satellites offer valuable insights into atmospheric CO emissions. However, these instruments differ in several aspects including sampling regime, pixel size, instrumental technology, and retrieval scheme. Understanding the discrepancies and agreements among these instruments is crucial for accurate interpretation, ensuring the reliable use of the observations for quantifying emission inventories and informing policy decisions. Reconciling the differences between the instruments is also important since the use of multiple data sets in any analysis increases the

robustness of the results. This study focuses on the comparability of retrieved CO measurements from MOPITT, IASI, and TROPOMI, in the context of wildfire conditions, particularly in September 2020 across North America.

The paper is structured as follows: Section 2 introduces the satellite data utilized in this study. In Section 3.1, we conduct a regional analysis of CO levels over the North American domain in September 2020. Section 3.2 presents the analysis of MOPITT and IASI daily CO profiles, followed by a detailed analysis of a case study in Section 3.3. Section 3.4 presents the analysis of contrasting regions. Finally, Section 4 provides a summary of the study and suggestions for future research.

## 2. Data

### 2.1. MOPITT

MOPITT is a nadir-viewing gas correlation radiometer that was launched in 1999 on board the NASA Earth Observing System (EOS)/Terra satellite to measure atmospheric CO. Terra is in a sun-synchronous orbit at an altitude of  $\sim 700$  km, with an equator crossing at  $\sim 10:30$  LT (local time) each morning and evening. The MOPITT instrument has a swath width of  $\sim 640$  km that makes approximately 14–15 orbits per day and it achieves near-global coverage every 3–4 days with a spatial resolution of  $22 \times 22$  km<sup>2</sup> (Drummond et al., 2022). MOPITT products have been consistently validated using ground-based remote sensing and aircraft data (Buchholz et al., 2022; Deeter et al., 2012, 2013, 2019; Emmons et al., 2002, 2004).

MOPITT is the only space-based instrument deriving CO simultaneously from near-infrared (NIR, 2.3- $\mu$ m), thermal infrared (TIR, 4.7- $\mu$ m), and multispectral radiances (TIR + NIR). TIR radiances are most sensitive to CO in the middle and upper troposphere, with better sensitivity over regions with greater thermal gradients such as deserts (Deeter et al., 2011). Since NIR retrievals depend on reflected solar radiation, observations are limited to daytime over land. Additionally, the NIR data exhibit approximately uniform sensitivity throughout the troposphere. The MOPITT joint (TIR/NIR) CO retrieval product provides improved sensitivity to CO in the lower troposphere compared to the TIR-only product (Deeter et al., 2011, 2012, 2013; Worden et al., 2010).

MOPITT CO retrieval products are generated using an iterative optimal estimation algorithm (Rodgers, 2000) involving both MOPITT calibrated radiances and a priori CO data (Deeter et al., 2003) under cloud-free conditions. The MOPITT retrieval algorithm is described in detail by Deeter et al. (2019) and Worden et al. (2013). It uses a priori CO profiles that are derived from a model climatology which varies seasonally and geographically (Deeter et al., 2003; Lamarque et al., 2003). The MOPITT products consist of the volume mixing ratio (VMR) of CO profiles on 10 vertical layers from the surface to 100 hPa which are integrated to provide the total column (TC) amounts (Deeter et al., 2003, 2014, 2017).

The MOPITT V9 product exhibits enhanced observational coverage, particularly during extreme pollution events, when compared to previous versions (Deeter et al., 2022; Marey et al., 2022). We use V9, Level-2 CO profiles, and TC CO retrievals of TIR and Joint (NIR + TIR) data over land and/or ocean scenes, depending on the region of interest.

### 2.2. IASI

IASI is a Fourier transform infrared spectrometer (FTS) that detects the TIR radiation emitted by the earth and the atmosphere, between 645 cm<sup>-1</sup> and 2,760 cm<sup>-1</sup>, with a spectral resolution of 0.5 cm<sup>-1</sup>. There are three IASI instruments on board the Metop sun-synchronous satellites: IASI-A, B, and C, launched in 2006, 2012, and 2018, respectively. IASI sensors view the ground through a cross-track rotary scan mirror with a horizontal resolution of 12 km at nadir, which increases at larger viewing angles (Clerbaux et al., 2009; Turquety et al., 2009). Each IASI instrument scans the atmosphere with a swath width of 2,200 km which achieves global coverage twice daily at 09:30 LT (Clerbaux et al., 2009).

IASI provides information on the atmospheric concentrations of several trace gases such as O<sub>3</sub> (Barret et al., 2011; Boynard et al., 2016), CO (George et al., 2009) and N<sub>2</sub>O (Barret et al., 2021), but in this study, we will be using level 2 CO profiles and TC observations (<https://iasi.aeris-data.fr/co/>, last access: 20 December 2021). The nadir spectral radiance in the range of 2143–2181.25 cm<sup>-1</sup> is used to retrieve CO. The retrieval is based on the Fast Optimal Retrievals on Layers for IASI (FORLI) algorithm (Barret et al., 2024), using single a priori. The IASI CO product consists of retrieved VMR profiles in 19 fixed layers corresponding to vertical layers of 1 km thickness

starting from the surface to 18 km. The last level represents a layer from 18 km to the top of the atmosphere (Clerbaux et al., 2009). IASI CO data are retrieved for a cloud fraction of less than 25% and have been validated against ground-based observations (Kerzenmacher et al., 2012), aircraft data (Klonecki et al., 2012; Pommier et al., 2010) and other satellite measurements (George et al., 2009). CO IASI data (Astoreca et al., 2021) that are utilized in this study were computed after filtering for Super Quality Flag (SQF) = 0 (see [https://iasi.aeris-data.fr/CO\\_readme/](https://iasi.aeris-data.fr/CO_readme/)).

### 2.3. TROPOMI

TROPOMI is a push-broom imaging spectrometer onboard the Sentinel-5 Precursor (S-5P) satellite that was launched on 13 October 2017. It is flying in a sun-synchronous orbit at 824 km altitude with a 13:30 LT Equator-crossing time. The TROPOMI grating spectrometer measures solar spectra reflected by Earth's surface in the UV–vis (270–500 nm), near-IR (675–775 nm), and the shortwave-infrared (SWIR) (2,305–2,385 nm) spectral bands. TROPOMI provides spectral measurements with daily global coverage with a swath of 2,600 km and a spatial resolution at nadir up to  $5.5 \times 7.0 \text{ km}^2$  in the SWIR (updated from  $7.0 \times 7.0 \text{ km}^2$  in August 2019).

TROPOMI CO data are processed with the Shortwave Infrared CO Retrieval (SICOR) algorithm that was developed for Copernicus operational data processing (Landgraf et al., 2016). The SICOR algorithm is based on a scattering forward simulation that retrieves cloud properties together with trace gas columns. The inversion deploys a profile-scaling approach (Borsdorff et al., 2014) where a CO reference profile is scaled to fit the TROPOMI reflectance measurements based on monthly averaged ( $3^\circ \times 2^\circ$ ) vertical CO a priori profiles from the TM5 chemical transport model (Krol et al., 2005). It provides total vertical column measurements of CO retrieved from the SWIR measurements, for clear-sky and cloudy conditions over land and for cloudy conditions over the ocean. Under clear-sky conditions over oceans, the signal is too low due to the dark sea surface in the SWIR to give a meaningful retrieval. The high reflectance of the cloud enables retrieval over the ocean.

The SICOR algorithm consists of two steps. In the first step, the SICOR algorithm (the forward simulation) retrieves the total amount of  $\text{CH}_4$  from the TROPOMI radiances between 2,315 and 2,324 nm to filter optically thick clouds and aerosols assuming a non-scattering atmosphere (Borsdorff et al., 2017). A full-physics algorithm retrieves CO in the second step from radiances between 2,324 and 2,338 nm. The  $\text{CH}_4$  retrievals from the first step are used to derive the effective cloud parameters (i.e., cloud optical thickness and cloud center height). A detailed outline of all settings for the CO retrieval for example, spectral windows, priori profiles, and other auxiliary data are given by Landgraf et al. (2016).

One of the advantages of the SICOR algorithm is that it provides retrievals for cloudy conditions using the sensitivity of the measurement to the CO above the cloud. The TROPOMI CO TC data sets include total-column averaging kernels (AVKs) for individual measurements that describe the vertical sensitivity of the retrieved CO columns. The CO retrieval under clear-sky atmospheric conditions has good sensitivity throughout the atmosphere, with minor variations due to the observation geometry of the satellite. The AVKs provided for individual retrievals under cloudy atmospheric conditions indicate the sensitivity loss resulting from shielding by clouds (Borsdorff et al., 2018).

The TROPOMI CO data set was validated with TCCON (Total Carbon Column Observing Network) measurements to show that the data set fulfills the mission requirements (10% precision and 15% accuracy for single soundings). However, the measurements of the TCCON stations are located mainly in unpolluted remote areas that represent the CO background concentration (Borsdorff et al., 2018, 2022). The BBFLUX (Biomass Burning Fluxes of trace gases and aerosols) team conducted an intercomparison of TROPOMI CO with airborne measurements under high aerosol loads from wildfires. By using FLEXPART simulations to account for the time mismatch of the TROPOMI and airborne measurements, in addition to accounting for the TROPOMI AVKs, they showed that TROPOMI CO was +9.0% systematically higher for the operational product (+7.4% for the scientific product) relative to the aircraft measurements. They showed that the TROPOMI CO product can be used to evaluate global wildfire emission fluxes with careful consideration taken for background corrections, ground pixel size, and atmospheric variability (Rowe et al., 2022).

For this study, we use TROPOMI offline Version 1.03.02 data (Apituley et al., 2020), which were downloaded through the Copernicus Open Access Hub (<https://s5phub.copernicus.eu/dhus/#/home>). TROPOMI quality assurance has four discrete levels: 0, 0.4, 0.7, and 1, which are based on Aerosol optical depth (AOD) and cloud

**Table 1**  
*TROPOMI Quality Flag Description*

Quality flag	Criteria	Condition
1	AOD < 0.5 and CL < 500 m	clear-sky and clear-sky like observations
0.7	AOD ≥ 0.5 and CL < 5,000 m	mid-levels cloud
0.4	AOD ≥ 0.5 and CL ≥ 5,000 m) or AOD ≤ 0.5 and CL ≥ 500 m)	high clouds, experimental data set
0	SZA > 80° or defective product	corrupted or defective data

height (CL) criteria (<https://sentinels.copernicus.eu/documents/247904/3541451/Sentinel-5P-Carbon-Monoxide-Level-2-Product-Readme-File>). The definition for each quality flag (qf) is given in Table 1 (Landgraf et al., 2016). Note: In later versions of the TROPOMI retrieval qf is a continuous variable in contrast with these discrete values. In this study, we limit the analysis to scenes under clear-sky (qf = 1) and few-cloud (qf = 0.7 and 1) atmospheric conditions.

Additionally, the Aerosol Index (AI) product retrieved by S5P TROPOMI is utilized in this study. AI is a qualitative index that measures the presence of aerosols with considerable absorption properties. AI is a measure of the occurrence of aerosols in the atmosphere, which is calculated using the 354 nm/388 nm wavelength pair (Torres et al., 2020). The wavelengths used have low ozone absorption, so unlike aerosol optical thickness measurements, AI can be calculated in the presence of clouds. AI values can be positive or negative. The magnitude of the aerosol AI signal (which range in values from a slightly negative background to values as high as 15) depends mainly on AOD, aerosol height, and aerosol absorption features (carbonaceous aerosol) (Torres et al., 2013). The positive AI values (range from 1 up to 15) indicate the presence of elevated absorbing aerosols which can be desert dust and biomass-burning aerosols. In contrast, the negative AI values indicate non-absorbing aerosols (Pandey, 2022).

#### 2.4. CALIOP

CALIOP is a polarization lidar instrument onboard the CALIPSO satellite which was launched in April 2006. The CALIPSO satellite is in a 705-km sun-synchronous polar orbit with a 16-day repeat cycle, with an overpass time of around 01:30/13:30 local solar time at the equator. It measures the total attenuated backscatter of aerosols at 532 and 1,064 nm providing detailed atmospheric vertical structure (Vaughan et al., 2004; Winker et al., 2009). It can observe both daytime and night-time aerosol and cloud backscatter profiles from the sea level to ~30 km (Winker et al., 2006; Kim et al., 2018). Backscattered signals are sampled at a vertical resolution of 30 m below 8.2 km altitude and 60 m between 8.2 and 20.2 km altitude. The diameter of CALIOP laser footprints on the ground is 70 m, with a 333-m horizontal spacing between footprint centers along the ground track (Kittaka et al., 2011; Winker et al., 2007). The latest CALIPSO data products are available from the Langley Atmospheric Science Data Center. In this study, CALIPSO Version 4.11 aerosol products were used (<https://www.earthdata.nasa.gov/learn/find-data>).

#### 2.5. Gridding and Collocation Methods

In this paper, the data were gridded into  $0.25^\circ \times 0.25^\circ$  bins. Each of the satellite instruments have different observational coverage as described above, but all the instruments were operating continuously through the period considered for the study. The data were collocated using the following three consecutive steps.

1. Gridding the CO TC data into  $0.25^\circ \times 0.25^\circ$  bins for daytime and nighttime each day in September.
2. Retention of the data in each bin and day if all three instruments have observations in that bin on that day.
3. Temporally averaging of the data over September 2020 for the spatial analysis or spatially averaging of the data over certain regions for the temporal analysis.

### 3. Results and Discussion

#### 3.1. Spatiotemporal Distribution of Atmospheric CO Observations

In this section, we investigate the spatial distribution of atmospheric CO concentrations during the September 2020 wildfire season. Figures 1a–1e show the gridded spatial variations of daytime TC CO over North America

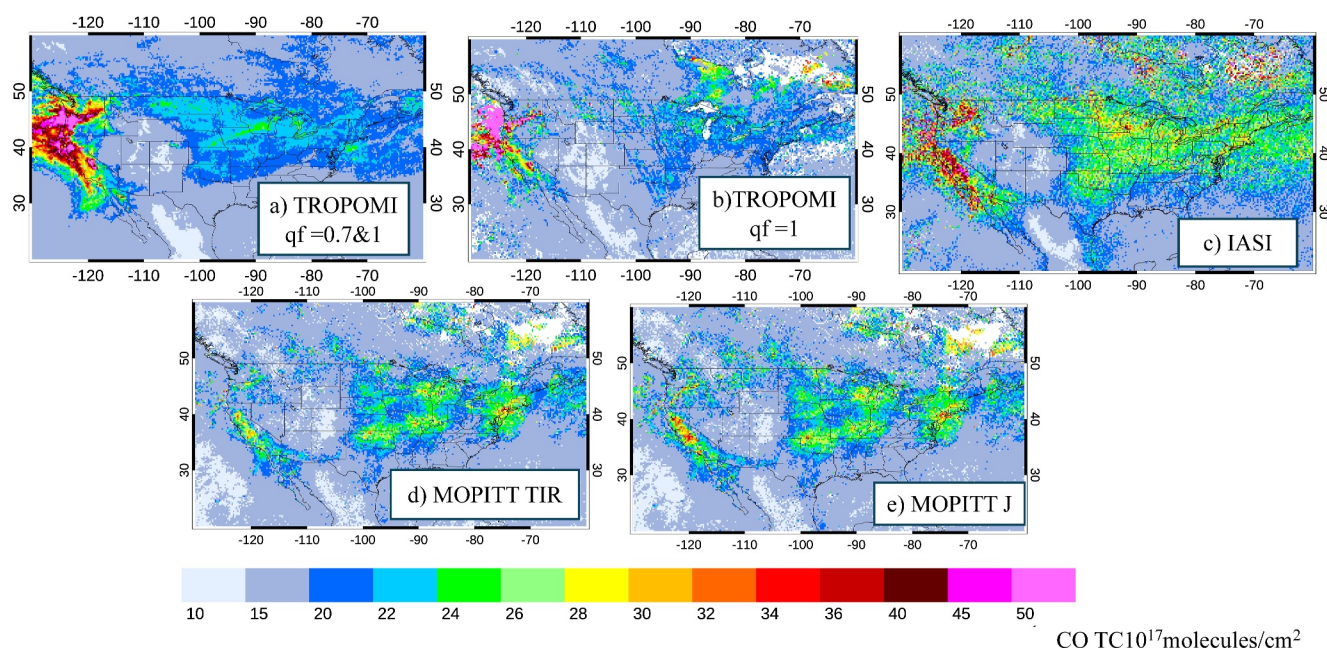


**Figure 1.** Spatial variations of non-collocated CO Total Column of TROPOMI data with  $qf > 0.7$  (a), TROPOMI data with  $qf = 1$  (b), IASI (c), MOPITT TIR (d), and MOPITT Joint (e), for September 2020. The data were gridded on a  $0.25^\circ \times 0.25^\circ$  grid.

(NA) from TROPOMI with  $qf = 0.7, 1$  (low cloud + clear) and  $qf = 1$  (clear), IASI, and MOPITT TIR-only and MOPITT J (joint retrieval). The CO total columns from all data sets exhibit a similar pattern over North America, with significant enhancements over both the eastern and western regions of the United States. Notably, TROPOMI shows prominent high CO levels in the Western U.S. region, whereas IASI and MOPITT display comparable values for both the western and eastern regions. The elevated CO values in the western region are associated with a series of wildfires that extended across eastern Washington state and southward into western Oregon and northern California. The fires commenced on 7 September 2020 and continued until around October 2020 (Abatzoglou et al., 2021; Albores et al., 2023; Mass et al., 2021; Reilly et al., 2022). The high CO values in the central and eastern regions of the US are a result of transported CO from the fires (Albores et al., 2023). Topography (higher elevation regions) affects (Dillon et al., 2011) the spatial distribution of CO TC where all data sets exhibit lower values in the Intermountain West.

The spatial distribution of atmospheric CO concentrations during the September 2020 wildfire season over North America was influenced by various factors, including topography, atmospheric dynamics, and synoptic-scale weather patterns (Nakata et al., 2022). High-elevation regions, such as those in the Intermountain West with valleys and basins surrounded by mountains, significantly impacted CO pollutant dispersion, acting as traps for pollutants and resulting in elevated CO TC values. Mountains obstructed air mass movement, creating localized pollution hotspots on the windward side and lower CO TC values on the leeward side (Dillon et al., 2011). Furthermore, the presence of high-amplitude mountain waves generated strong easterly winds over western Oregon, further influencing pollutant dispersion and facilitating rapid wildfire spread, particularly in the Oregon Cascades. The strong easterly winds observed in September 2020, particularly over the Pacific Northwest, exacerbated wildfire activity, emphasizing the crucial role of atmospheric dynamics in wildfire behavior and pollutant dispersion (Mass et al., 2021; Reilly et al., 2022). Thus, there would be a reduced amount of CO in the atmosphere above these areas compared to regions at lower elevations (e.g., in regions between  $110^\circ\text{--}100^\circ\text{W}$  and  $30^\circ\text{N}\text{--}40^\circ\text{N}$ ).

Finally, regions with higher elevations theoretically would exhibit lower CO TC values due to smaller air column mass. Elevated CO values were evident in both western and eastern regions, contrasting with lower concentrations observed around  $110^\circ\text{--}100^\circ\text{W}$  and  $30^\circ\text{--}40^\circ\text{N}$ . Overall, the complex interaction among topography, atmospheric dynamics, synoptic-scale weather patterns, and vegetation characteristics contributed to shaping spatial

variations in atmospheric CO concentrations during the September 2020 wildfire events (Mass et al., 2021; Reilly et al., 2022; Russell et al., 2024).

While IASI and TROPOMI CO exhibit higher CO values over the Western U.S. relative to MOPITT, MOPITT and IASI display higher values over Hudson Bay (HB) and the central and eastern U.S. compared to TROPOMI. Also, the MOPITT and IASI CO TC data demonstrate more consistency over the eastern U.S., with higher values relative to TROPOMI. However, MOPITT CO TC has less coverage and a larger pixel size than IASI, resulting in MOPITT showing CO levels over broader regions. In contrast, IASI can capture finer variations and has more coverage.

Several factors could lead to differences in the observed CO between the three satellite measurements. First is the Equator-crossing time of the instrument. TROPOMI has a cross time of 13:30, whereas for MOPITT it is at 10:30 and 22:30, and for IASI it is at 09:30 and 21:30. Morning measurements by MOPITT and IASI capture CO concentrations influenced by overnight transport and mixing processes, while TROPOMI's afternoon measurements reflect the accumulation of pollutants throughout the day. These differences in measurement timing between afternoon (for TROPOMI) and morning (for MOPITT and IASI) can lead to variations in observed CO values due to diurnal fluctuations, and differences in transport and dispersion patterns (Busa et al., 2022). During the September 2020 wildfires in the western US, diurnal variations in CO TC can be expected to mirror the dynamics of the fires and atmospheric conditions. Wildfires tend to be more active during the daytime due to factors such as higher temperatures, increased solar radiation, and stronger winds, resulting in peak CO emissions during the late morning to afternoon hours. Although wildfires may continue to burn at night, their intensity typically diminishes compared to daytime, leading to lower CO emissions and concentrations in the early morning hours. Furthermore, the transport and dispersion of smoke plumes and CO emissions vary throughout the day because of changes in wind patterns and atmospheric boundary layer dynamics. These variations contribute to spatial differences in CO TC values, with downwind areas experiencing higher levels during specific times of the day (Andreae & Merlet, 2001).

Second is the treatment of clouds in the field-of-view. The TROPOMI retrieval algorithm retrieves CO under both clear and cloudy conditions, whereas IASI CO data are retrieved for a cloud fraction of less than 25% (Clerbaux et al., 2009) and MOPITT CO data are retrieved with a cloud fraction of less than 5% (Deeter et al., 2021; Marey et al., 2022). For many cloud-clearing regimes in high aerosol locations, aerosol can be flagged as clouds.

Third is the wavelength at which the measurements are made. TROPOMI measures in the NIR range (~2,350 nm), utilizing reflected solar radiation to estimate CO levels, which is sensitive to atmospheric scattering and absorption effects. In contrast, IASI measures CO in the TIR range (~4,700 nm), relying on thermal radiation emitted by Earth's surface and atmosphere, which is sensitive to the atmospheric temperature and emissivity. Additionally, TIR measurements are influenced by surface temperature contrast, which affects the retrieval of atmospheric composition information. The TIR measurements usually provide up to two independent pieces of information, rather than a complete vertical profile. MOPITT's joint product takes advantage of both wavelengths, allowing for complementary information on CO distribution and concentration (Borsdorff et al., 2014; Clerbaux et al., 2009; Veefkind et al., 2012; Worden et al., 2010).

Fourth is the different spatial resolution and swath widths of the measurements. MOPITT has a significantly smaller swath than IASI or TROPOMI which leads to lower temporal resolution. TROPOMI has the smallest pixel size ( $5.5 \times 7.0 \text{ km}^2$ ), followed by IASI (12 km diameter), and then MOPITT ( $22 \times 22 \text{ km}^2$ ).

Fifth and finally, the retrieval approaches are different as discussed in Section 2 above (Borsdorff et al., 2014; Clerbaux et al., 2009; Deeter et al., 2007; Veefkind et al., 2012).

To account for some of these factors, we collocated the CO TC data (see Section 2.5 above) and the results are shown in Figure 2. The collocated values over the HB region, and the central and eastern US regions are in better agreement across all three instruments. However, over the western region, the IASI and TROPOMI values are higher than the corresponding MOPITT TIR and Joint observations. While the collocation approach considers data within the same bin, it is worth noting that TROPOMI's smaller footprint allows for more effective sampling of smaller-scale features like smoke plumes, potentially resulting in higher TC CO (TCO) values even within the  $0.25^\circ \times 0.25^\circ$  grid. Hence, due to the varying spatial resolutions among the instruments, the spatial information captured within each collocated grid cell may differ. If an area has partial cloud or smoke obscuration, a higher resolution measurement may find clear areas whereas the lower resolution measurement may mask these areas as



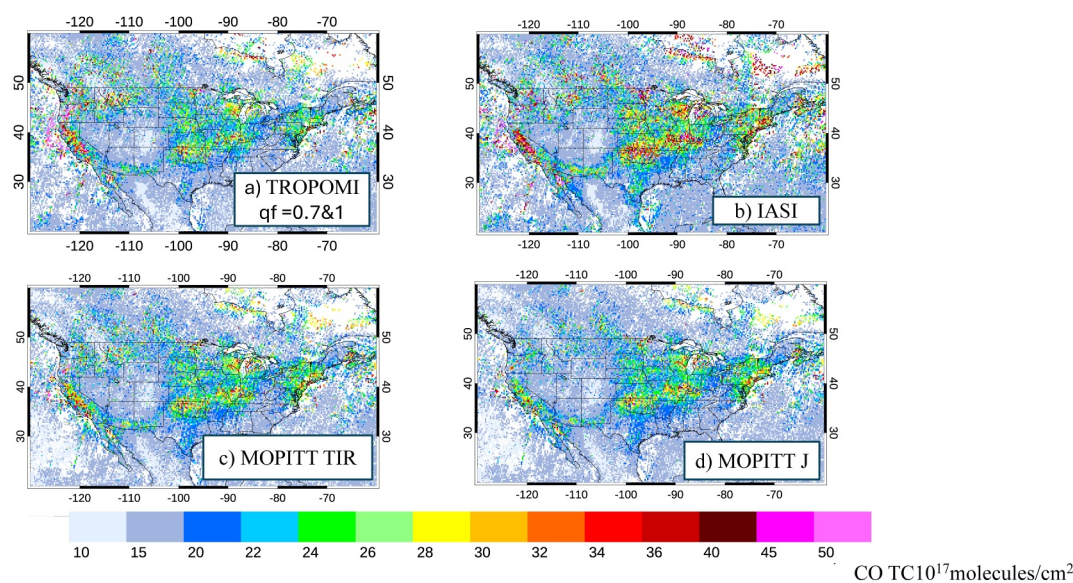


**Figure 2.** Spatial variations of collocated CO Total Column of TROPOMI data with  $qf > 0.7$  (a), IASI (b), MOPITT TIR (c), and MOPITT Joint (d), for September 2020. The data were gridded on a  $0.25^\circ \times 0.25^\circ$  grid.

cloudy, resulting in fewer data points due to the coarse resolution. This difference in spatial coverage can influence overall TCO measurements and contribute to discrepancies among the instruments. Therefore, when comparing TCO values across instruments, it is crucial to consider both spatial resolution and coverage.

We selected the following four regions for a time series analysis to examine the daily variations of CO: North America (NA), HB, the central and eastern U.S. (CEUS), and the Pacific Northwest (PNW). The boundaries of the four selected regions are given in Table 2 and the time series for the regions are shown in Figure 3. Data from TROPOMI ( $qf = 0.7$  and 1, cloudy and clear), IASI, and MOPITT (TIR and Joint products) were separated for day and night conditions. In the North American domain (Figure 3a), the daily mean time series for the three instruments exhibit a similar overall pattern, characterized by low CO values at the beginning and end of the month and a peak in the middle of the month. Generally, all sensors show good agreement at low CO values (typical CO TC levels), however, they exhibit larger discrepancies when CO values are high. For instance, between September 10–25, notable discrepancies arise at certain times, with differences that can exceed 50%. Looking at the time series of the non-collocated data (Figure 3a, left side), on September 13th, MOPITT TIR nighttime data (black) records a value of approximately  $1.5 \times 10^{18}$  molecules/cm<sup>2</sup>, while IASI nighttime data (pink) show a value of around  $2.6 \times 10^{18}$  molecules/cm<sup>2</sup>. On September 15, IASI daytime observations (orange) show a value of around  $3.3 \times 10^{18}$  molecules/cm<sup>2</sup>, while MOPITT J and TROPOMI data record TC CO values of around  $2.5 \times 10^{18}$  molecules/cm<sup>2</sup>. With the collocated data (Figure 3a-right panel), CO TC values from the three sensors are more consistent with the highest values from IASI and the lowest values from the MOPITT TIR data.

All the regions experienced several fire-driven CO peaks between September 8–25. However, these peaks differed in terms of timing, frequency, and intensity. The peaks were most prominent over the CEUS (Figure 3c) and PNW regions (Figure 3d), while the HB region only experienced one peak between 20 and 25 September

(Figure 3b). In the non-collocated data (Figure 3b-left), the highest CO TC values were observed for daytime from IASI ( $4.5 \times 10^{18}$  molecules/cm<sup>2</sup>) followed by TROPOMI ( $4 \times 10^{18}$  molecules/cm<sup>2</sup>), and MOPITT J ( $2.8 \times 10^{18}$  molecules/cm<sup>2</sup>). However, during the nighttime, the CO TC values were slightly lower, with IASI recording  $3.5 \times 10^{18}$  molecules/cm<sup>2</sup> and MOPITT TIR recording  $2.5 \times 10^{18}$  molecules/cm<sup>2</sup>. In contrast, the collocated data (Figure 3b-right) showed the highest CO TC values for nighttime IASI and MOPITT, with values of  $4 \times 10^{18}$  and  $3 \times 10^{18}$  molecules/cm<sup>2</sup>, respectively. It is reasonable to attribute this late CO peak to long-range transport from the PNW fires. MODIS AOD (not shown) also indicates high

**Table 2**  
The Boundaries of the Four Selected Regions for the Daily Time Series

Region	Latitude	Longitude
NA	35°–60°N	60°–130°W
HB	50°–60°N	80°–95°W
CEUS	34°–46°N	80°–100°W
PNW	35°–48°N	115°–130°W

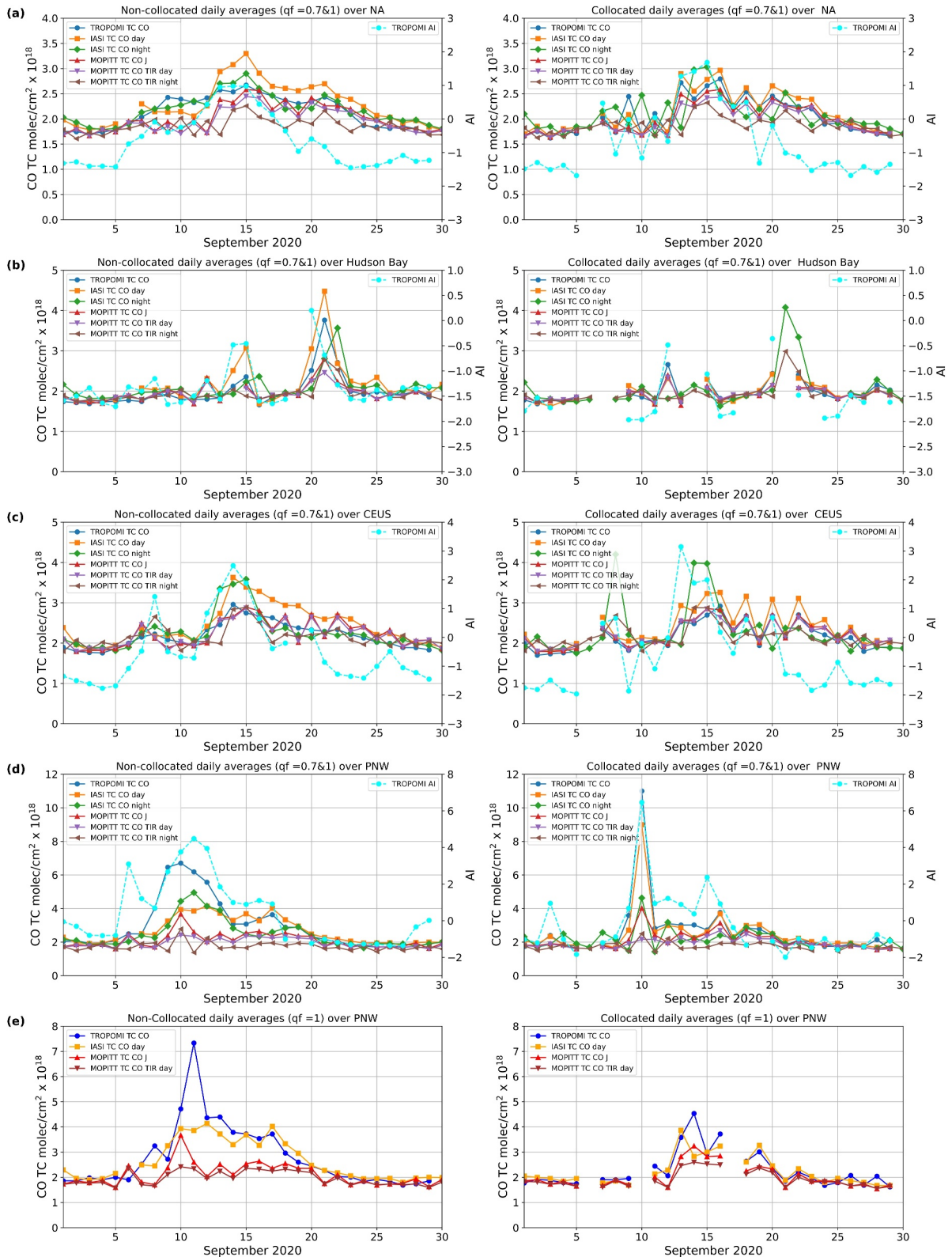


**Figure 3.** Daily time series of Measurements of Pollution in the Troposphere, Infrared Atmospheric Sounding Interferometer and Tropospheric Monitoring Instrument averaged over (a) North America, (b) Hudson Bay, (c) CEUS and (d) and (e) PNW for  $qf \geq 0.7, 1$  on September 2020. The left panels show the time series of all (non-located) of the available observations (after quality assurance filtering), while the right panels contain the time series of only the collocated data. TROPOMI AI data are plotted in cyan, with AI values (unitless) indicated on the right y-axis.

values over HB during the same time. The high aerosol levels are consistent with the eastward and northward transport of the biomass burning smoke as indicated by true-color images on September 20th (Figure S1a in Supporting Information S1).

During wildfire events, smoke plumes containing aerosols and pollutants can be injected into the upper troposphere and even the lower stratosphere by strong convective updrafts associated with the fires. Once in the upper atmosphere, these emissions can be transported horizontally by high-altitude winds, such as the jet stream, over large distances (Russell et al., 2024; Wilmot et al., 2022). Measurements from CALIPSO were utilized to monitor the height of the smoke plumes. Figure S1a in Supporting Information S1 illustrates true-color images from September 20th overlaid with the trajectory of CALIPSO as it traversed over HB during nighttime on 20 September 2020. Figure S1b in Supporting Information S1 shows the vertical distribution of the aerosol backscatter coefficient recorded by CALIPSO on the same date (for the yellow path). It indicates that the plume height ranged from 5 to 10 km, consistent with the intercontinental transport of the smoke.

The temporal variations observed in the CEUS region (as depicted in Figure 3c) are indicative of the potential influence of emissions transported from the Western U.S. fires. This inference is supported by the prevailing westerly mean wind in the free troposphere, particularly at around 750 hPa, during September 2020, as reported by Albores et al. (2023). The magnitude of CO TC values over the CEUS region (Figure 3c, left panel) in the non-collocated daytime data shows that IASI recorded the highest CO TC value of  $3.5 \times 10^{18}$  molecules/cm<sup>2</sup>, while TROPOMI and MOPITT measured a maximum of approximately  $3 \times 10^{18}$  molecules/cm<sup>2</sup>. During nighttime, IASI recorded the highest values of  $3.5 \times 10^{18}$  molecules/cm<sup>2</sup>. Conversely, in the collocated daytime data (Figure 3c, right panel), IASI registered the highest CO TC value of  $4.5 \times 10^{18}$  molecules/cm<sup>2</sup>. In the collocated nighttime data, IASI recorded the highest value of  $4 \times 10^{18}$  molecules/cm<sup>2</sup>. In all cases, the MOPITT TC values showed a maximum of about  $3 \times 10^{18}$  molecules/cm<sup>2</sup>. Our results are consistent with Albores et al. (2023), who observed a significant increase in background pollution levels across the entire North American domain because of fire emissions transported from the western part of the U.S.

The CO TC maximum in all the regional subsets did not exceed  $5 \times 10^{18}$  molecules/cm<sup>2</sup>, except in the PNW (see Figure 3d, but note that the y-axis scale is different) which experienced a strong peak between 8 and 15 September. The PNW TROPOMI CO TC values of non-collocated (all data) increased to  $6.5 \times 10^{18}$  molecules/cm<sup>2</sup> and the collocated data for TROPOMI and IASI exceeded  $8 \times 10^{18}$  molecules/cm<sup>2</sup>. These extremely high values reflect the contribution of Western U.S. fires to the total CO (Abatzoglou et al., 2021; Albores et al., 2023; Mass et al., 2021; Varga et al., 2022).

In the PNW region (Figure 3d), the IASI and TROPOMI data exhibit significant discrepancies relative to MOPITT when CO TC levels are extremely high, specifically for the second week of September. On 10 September 2020, the left panel (all data, not co-located) showed high values in the TROPOMI, IASI, and MOPITT Joint CO data. However, the TROPOMI magnitude is  $6\text{--}7 \times 10^{18}$  molecules/cm<sup>2</sup>, much higher than the IASI and MOPITT Joint CO data that have values around  $4\text{--}5 \times 10^{18}$  molecules/cm<sup>2</sup>, and the MOPITT TIR data with values of about  $2.5 \times 10^{18}$  molecules/cm<sup>2</sup>. Following this peak on 10 September 2020, the MOPITT (both Joint and TIR) CO values decreased to  $\sim 2 \times 10^{18}$  molecules/cm<sup>2</sup>, while the IASI and TROPOMI values remained high until about 18 September. This behavior could be attributed to differences in the temporal and spatial sampling density between the sensors. The MOPITT temporal resolution of about 3 days could account for less sampling of the fire CO emission compared to IASI and TROPOMI (with daily temporal resolution). The less frequent sampling of MOPITT compared to IASI and TROPOMI means that MOPITT might not capture the full range of short-term variations in CO concentrations, particularly during intense fire events when CO emissions can peak rapidly and then decrease. This lower temporal resolution of MOPITT could lead to underestimation or smoothing of CO concentrations, resulting in lower observed values compared to instruments with higher temporal resolution like IASI and TROPOMI.

The collocated data (Figure 3d, right panel) on 10 September 2020 show substantial discrepancies, with IASI and TROPOMI values greater than  $8 \times 10^{18}$  molecules/cm<sup>2</sup>, about double the CO values in the MOPITT Joint data. While the non-collocated data (Figure 3d, left panel) might exhibit discrepancies due to differences in temporal sampling, the variations between MOPITT and the other instruments in the collocated data set (Figure 3d, right panel) suggest that factors beyond sampling frequency may contribute to these differences. These factors could encompass all of the five issues enumerated above. Thus, while temporal sampling frequency may influence non-collocated discrepancies, it is evident that additional factors play a role when examining collocated data.

Rowe et al. (2022) emphasized the significant effect of smoke aerosols on the CO retrievals. To assess the influence of high aerosol loading on the CO data, a similar time series of the daily AI from TROPOMI is displayed in Figure 3, on the right y-axis (cyan dashed). The high AI values (Figure 3d) coincide with the corresponding extremely high IASI and TROPOMI CO observations. The magnitude of the AI maximum over the PNW was approximately 4 for non-collocated (all data) and 7 for collocated data. These exceptionally high AI levels indicate heavy smoke aerosol loading (Torres et al., 2020) resulting from the wildfires in the western U.S. The observed correlation between the notably high TROPOMI CO levels and the AI data underscores the complex interactions between aerosols, trace gases, and measurement techniques, particularly in environments affected by wildfires. Elevated levels of aerosols, such as smoke particles from wildfires, can enhance the scattering of sunlight, leading to an increase in measured AI values. Furthermore, under conditions of high aerosol loading, multiple scattering of light within the atmosphere becomes more pronounced, amplifying the signals detected by TROPOMI, including the CO and AI measurements. These findings are consistent with earlier studies; for example, Juliano et al. (2022) documented persistent smoke plumes in the region during September 7–11, 2020, which had a significant impact on solar power generation in California, resulting in potential reductions of approximately 10%–30%.

Rowe et al. (2022) also suggested that under high aerosol load conditions, TROPOMI CO signals can be enhanced due to multiple scattering. According to their study, multiple scattering phenomena within these plumes can lead to an overestimation of vertical column densities (VCDs) observed by TROPOMI. Additionally, it is noted that TROPOMI retrievals for  $qf \geq 0.7$  (low cloud conditions) are sensitive to CO in slightly cloudy conditions, which might indicate the presence of smoke aerosols (Landgraf et al., 2016). This study shows such a potential relationship between the high TROPOMI CO levels and AI data. Although the TROPOMI CO retrieval process already incorporates a multi-scattering forward calculation to mitigate this issue, a more sophisticated model may be necessary to fully account for aerosol scattering effects, especially in scenarios involving optically thick smoke from wildfires.

Aerosol algorithms are designed to discriminate various atmospheric particles, including clouds and aerosols, in satellite imagery. However, during specific conditions, such as dust storms and biomass burning events, these algorithms may erroneously classify thick smoke plumes as clouds. This misclassification arises because both clouds and dense smoke plumes can exhibit similar traits in satellite observations, such as high reflectivity and opacity. Consequently, the algorithm might inaccurately interpret the smoke as clouds, leading to errors in analyzing atmospheric composition and air quality (Robbins et al., 2022). To isolate the influence of clouds that might result from thick smoke plumes, a daily time series of TROPOMI CO observations with  $qf = 1$  (clear conditions) is compared to the IASI and MOPITT time series over the PNW (Figure 3e). In the non-collocated data with  $qf = 1$  (Figure e-left), the intensity of the TC CO enhancements is generally lower than that of the corresponding data with  $qf \geq 0.7$  (0.7, 1) (Figure 3d, left panel), except on September 11th. However, in the collocated data with  $qf = 1$  (Figure 3e, right panel), the high CO peak observed on September 10th for the cloudy TROPOMI data (Figure 3d, right panel) is absent when flagging this area as cloudy. This result aligns with the argument that high aerosol levels can be misinterpreted as clouds in smoky conditions. Such misinterpretations can lead to missing the sampling and subsequently lower detected CO values due to smoothing averages (Deeter et al., 2022; Marey et al., 2022).

Thus, it suggests that the high TROPOMI CO signal is associated with dense smoke plumes. The absence of the high CO peak observed on September 10th for the cloudy TROPOMI data (Figure 3d, right panel) in the clear TROPOMI CO observations (Figure 3e) further supports this conclusion. To further explore the variations in the CO retrievals in smoke plumes, a case study during the Western U.S. wildfire season is presented in Section 3.3.

### 3.2. Analysis of MOPITT and IASI Daily CO Profiles

Figure 4a displays MOPITT and IASI collocated profiles over North America (NA), while Figure 4b illustrates the same profiles after filtering out data based on CO TC values greater than  $3 \times 10^{18}$  molecules/cm<sup>2</sup>, isolating fire pollution events from background/typical pollution conditions. It was observed that globally CO TC values do not exceed  $3 \times 10^{18}$  molecules/cm<sup>2</sup> unless there are severe pollution conditions (Parrish, D.D. et al., 2011; Emmons, L.K. et al., 2004).

The comparison of MOPITT TIR and IASI daily CO profiles is performed over the whole NA domain for September 2020. Data from both instruments are gridded in  $0.25^\circ \times 0.25^\circ$ , for each day in September then the

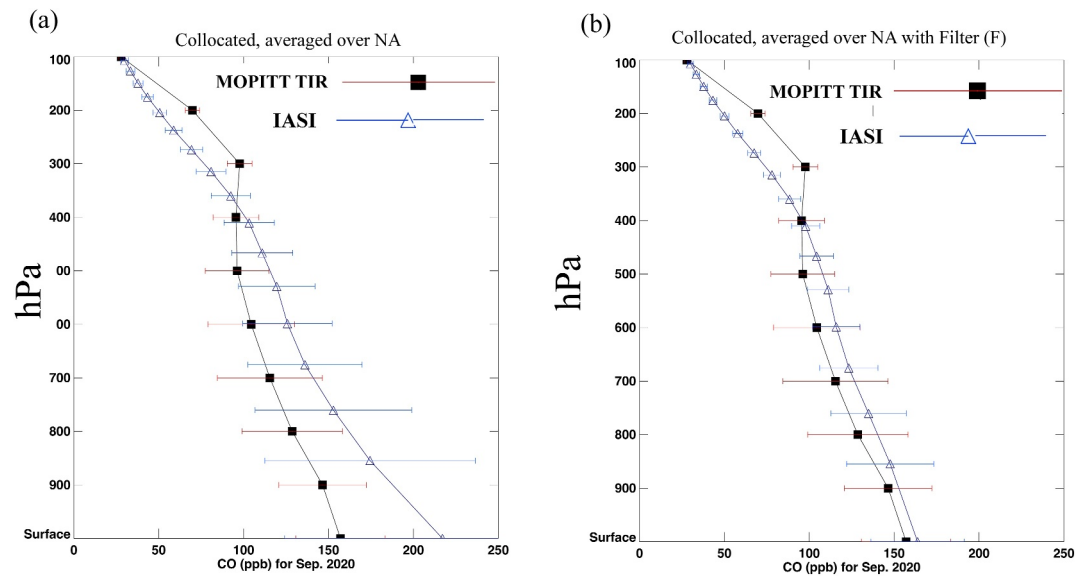


**Figure 4.** Mean Measurements of Pollution in the Troposphere and IASI daily CO profiles averaged over NA for September 2020. The profiles were calculated using the collocated data, however, data with CO total column (TC) values greater than  $3 \times 10^{18}$  molecules/cm<sup>2</sup> were omitted in the panel (b). “F” represents filtered data where CO TC values exceeding  $3 \times 10^{18}$  molecules/cm<sup>2</sup> have been omitted.

collocated profiles are averaged over the NA domain for all of September 2020. High CO concentrations are observed near the surface by the IASI instrument, with a mean of about 220 ppb, whereas the corresponding MOPITT TIR retrievals are about 150 ppb. These differences decrease in the middle to upper troposphere, typically around the 400 hPa level. However, with increasing altitude into the upper troposphere, the differences between MOPITT and IASI values begin to rise again and MOPITT has higher values compared to IASI, with the differences becoming comparable in magnitude to those observed in the middle to upper troposphere.

The retrieved CO profile is essentially a combination of the true atmospheric profile and the a priori profile, weighted by the AVK matrices. Moreover, errors associated with both the observation process and other parameters further contribute to the discrepancies (Rodgers, 2000). A crucial aspect of the retrieval process is the choice of the a priori profile, which comprises an expected profile and its associated covariance matrix, and which constrains the retrieved CO profile to fall within the range of physically realistic solutions (based on the known variability of this species).

IASI and MOPITT use different prior profiles in their retrievals. IASI utilizes a single prior (Clerbaux et al., 2009), while MOPITT relies on a climatology of the MOZART-4 chemistry transport model. For each retrieval, the climatology is spatially and temporally interpolated to match the date and location of the MOPITT observation (Deeter et al., 2017). For the covariance matrix, IASI retrievals exhibit greater variability around the prior, especially at the surface, leading to higher CO variations at the surface, whereas MOPITT retrievals tend to remain closer to the prior (Clerbaux et al., 2009). The MOPITT covariance matrix allows for a 30% variability in each retrieved layer (Deeter et al., 2010). In contrast, the IASI covariance matrix allows a maximum variability of 63% in the first layer, decreasing to 35% between 5 and 6 km, 30% between 6 and 10 km, and then increasing again, reaching 45% between 15 and 16 km (George et al., 2015; Turquety et al., 2009). This variability pattern reflects the nature of infrared (IR) radiative retrieval, which exhibits the greatest sensitivity in the middle troposphere. George et al. (2015) observed that IASI demonstrates better performance in capturing sudden spikes in CO levels during unexpected events. However, IASI's covariance matrix has larger values in the off-diagonal elements especially at lower altitudes, enabling it to adapt more effectively to rapid changes in atmospheric CO levels. George et al., 2015 found that MOPITT generally agrees better with aircraft profiles for observations with persisting high levels of CO throughout the year because of its climatology-based a priori, which closely approximates the actual atmospheric state except in situations of pollution or seasonal fire activity. Therefore, providing the retrieval with more freedom is beneficial during extreme events because these events are inadequately represented by any prior, even one like MOPITT's which includes some variability.

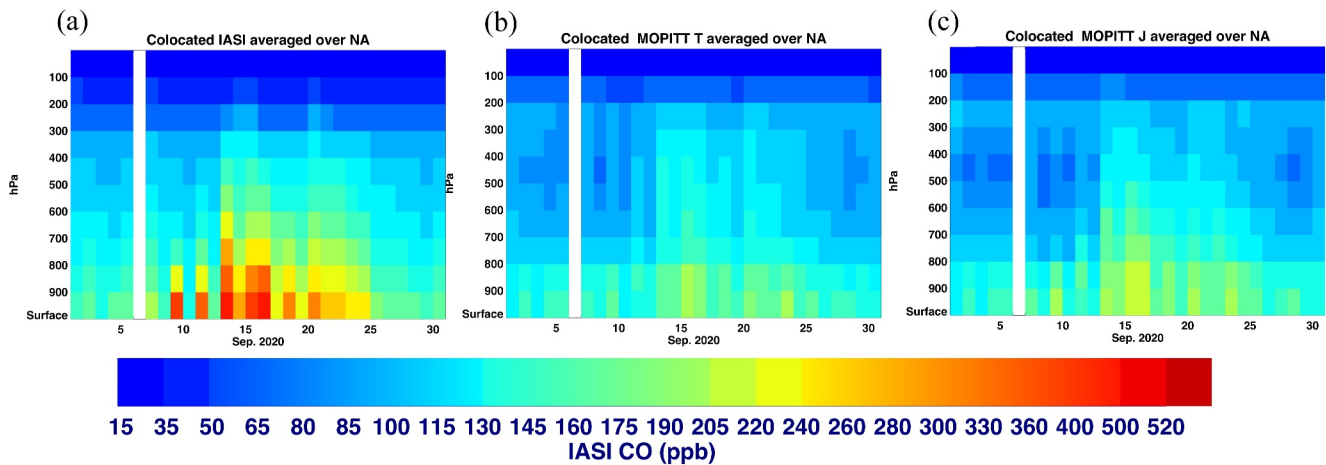


**Figure 5.** Time-altitude plots on September 2020 over the North American region of collocated (a) Infrared Atmospheric Sounding Interferometer profiles, (b) MOPITT TIR and (c) Measurements of Pollution in the Troposphere Joint profiles.

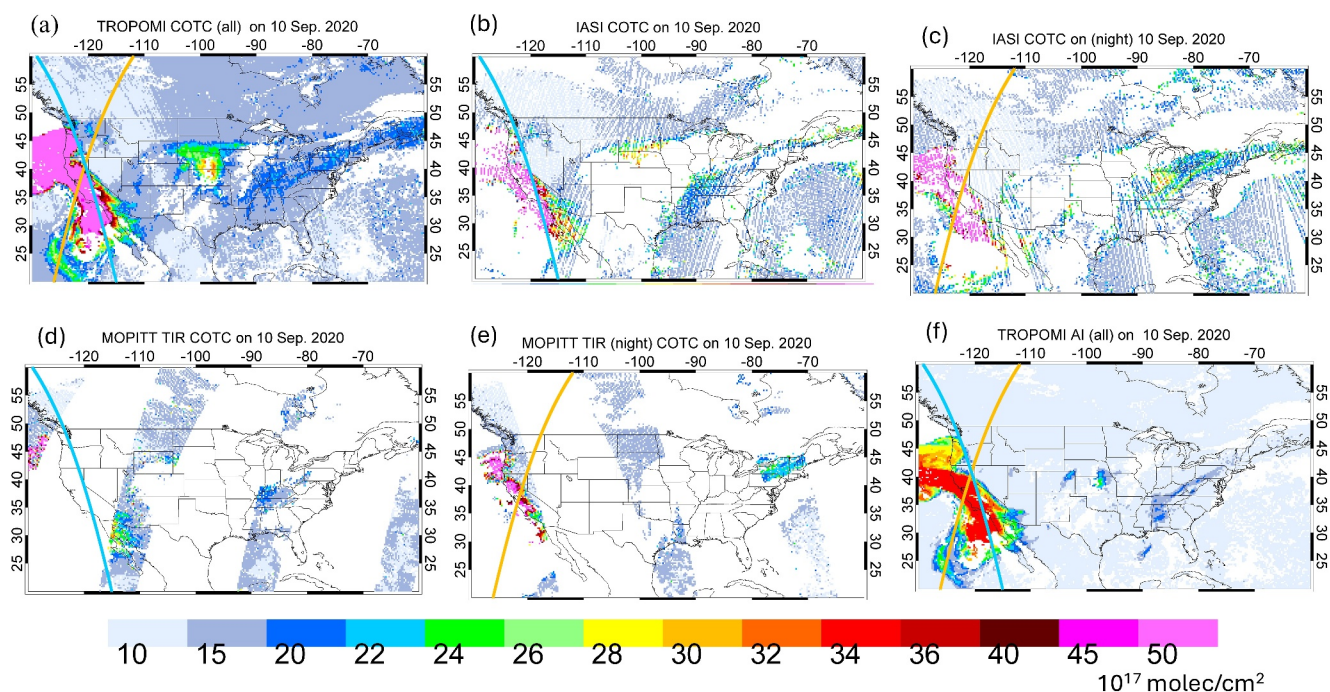
After removing the high CO TC data (values greater than  $3 \times 10^{18}$  molecules/cm<sup>2</sup>), the two data sets exhibit closer agreement within the error bars, as illustrated in Figure 4b. The improvement in agreement between the data sets is particularly evident in the lower to middle troposphere. However, differences persist in the upper troposphere, specifically between 400 and 200 hPa. George et al. (2015) stated that this disparity can be attributed to the larger sensitivity observed in this altitude range.

Figure 5a–5c show the daily collocated MOPITT Joint and IASI CO profiles over the whole NA domain in September 2020. They show that MOPITT is comparable to IASI in the upper troposphere and considerably lower in the middle and lower troposphere, especially during episodic fire event times. While the MOPITT Joint CO profiles exhibited higher concentrations near the surface compared to the corresponding TIR data, the IASI CO concentrations were approximately double (>500 ppb) those of the corresponding MOPITT Joint data during the fire episode. The high IASI values near the surface relative to the corresponding MOPITT values are probably the result of the different covariance matrices used in the retrievals. Additionally, a correlation exists between the surface and the middle troposphere, allowing the projection of information from layers with high sensitivity to layers where the sensitivity is weaker. Since the AVK indicates that the peak sensitivity of IASI is in the middle troposphere, it is expected that information from the middle troposphere layer is projected to the lower troposphere layer (George et al., 2015; Lutsch et al., 2022).

### 3.3. Case Study

Figure 3d displays the time series analysis of daily CO which shows extremely high values on 10 September 2020 over the PNW that is associated with the western wildfires. By 10 September, the smoke from the western Oregon fires had merged into a single dense smoke plume extending from the Cascade crest in northern California to southwestern Washington (Mass et al., 2021). We also further consider the satellite CO TC (MOPITT, IASI, and TROPOMI) and the TROPOMI AI along the CALIPSO path during day and night on 10 September 2020 (Figure 6). CALIPSO data of aerosol backscatter at 532 nm is used to investigate the atmospheric aerosol profile. Thus, in this section, a detailed analysis of CO TC derived from the three instruments along with TROPOMI AI will be conducted on 10 September 2020. Figure 6a–6f show the spatial variations of the TROPOMI CO, IASI CO (daytime and nighttime), MOPITT CO (daytime and nighttime), and TROPOMI AI data, respectively, over North America.

The TROPOMI and IASI CO TC in Figures 6a and 6b show substantial CO enhancement in the western region with values greater than  $6 \times 10^{18}$  molecules/cm<sup>2</sup>. The TROPOMI AI (Figure 6f) values exceed 8 with a similar spatial distribution to the TROPOMI CO distribution (Figure 6a). Both IASI daytime and nighttime maps reveal CO enhancements in the western region, with evidence of transport of CO over the Pacific Ocean coast. This coastal transport of CO across the ocean is evident in the MOPITT data, but MOPITT has less dense sampling and retrieves CO data only under clear conditions, resulting in low sampling over fire-affected regions. Note that



**Figure 6.** Spatial distribution on 10 September 2020 of (a) TROPOMI CO TC, (b) and (c) IASI CO TC for day and night, (d) and (e) MOPITT CO TC for day and night, and (f) TROPOMI AI. The cyan and yellow lines are the CALIPSO daytime and night track respectively.

heavy smoke aerosols can also sometimes be misinterpreted as clouds (Deeter et al., 2022; Marey et al., 2022). Due to these issues, it is anticipated that capturing the entire plume path with MOPITT may be challenging. The nighttime MOPITT (Figure 6e) and IASI (Figure 6c) data capture some of the CO from the western fire emissions, indicating that the fire emissions persisted for a relatively long time. Indeed, other studies have shown that the duration of the extraordinary September 2020 fire season spanned over two weeks (Evers et al., 2022).

Figure 7a shows the satellite CO TC and TROPOMI AI along the CALIPSO daytime track on 10 September 2020. There are two fire-driven peaks in CO, between 30°–40°N and 40°–50°N, whereas the nighttime data shown in Figure 7b exhibits only one peak, between 30° and 40°N. The two CO TC daytime peaks are about  $15 \times 10^{18}$  and  $6 \times 10^{18}$  molecules/cm<sup>2</sup>, which are associated with AI values of 14 and 14, respectively (Figure 7a). The IASI and TROPOMI CO TC peaks (daytime) follow the TROPOMI AI values, reflecting the potential smoke impact on the high CO retrieval values.

The magnitude of the aerosol AI signal depends mainly on AOD, aerosol height, and aerosol absorption features (carbonaceous aerosol) (Torres et al., 2013). The cause of the AI enhancements is possibly increased aerosol height and/or an enhanced aerosol absorption characteristic. The AI increases rapidly with AOD and aerosol height up to AOD of about 4. Large AI values are generally associated with large quantities of UV-absorbing aerosol particles in the upper troposphere and lower stratosphere (UTLS), such as wildfire-triggered pyro-cumulonimbus (pyroCb) episodes (Torres et al., 2020). Thus, high AI values effectively become a measure of aerosol height (Torres et al., 2020), which is consistent with the CALIPSO profiles (Figures 7d–7c). For example, the high altitude (~8 km) and dense aerosols that are seen in the daytime CALIPSO data (reds and greys in the color scale) coincide with the high TROPOMI AI values of around 14. Regarding the nighttime data, Figure 7b shows high IASI CO TC values that are consistent with the corresponding CALIPSO data, which suggest heavy aerosol loading (red color scale) at high altitudes (6–8 km). Nakata et al. (2022) suggested that the complex mountain topography of the region influenced the wind dynamics causing smoke to rise to high altitudes.

The consistent pattern observed between the high CO TC mirrors the findings of Rowe et al. (2022), who examined the TROPOMI CO measurements during a 2018 biomass-burning event, revealing TROPOMI's sensitivity to CO enhancements across wildfire plumes. By integrating simulations from the FLEXible PARTICle

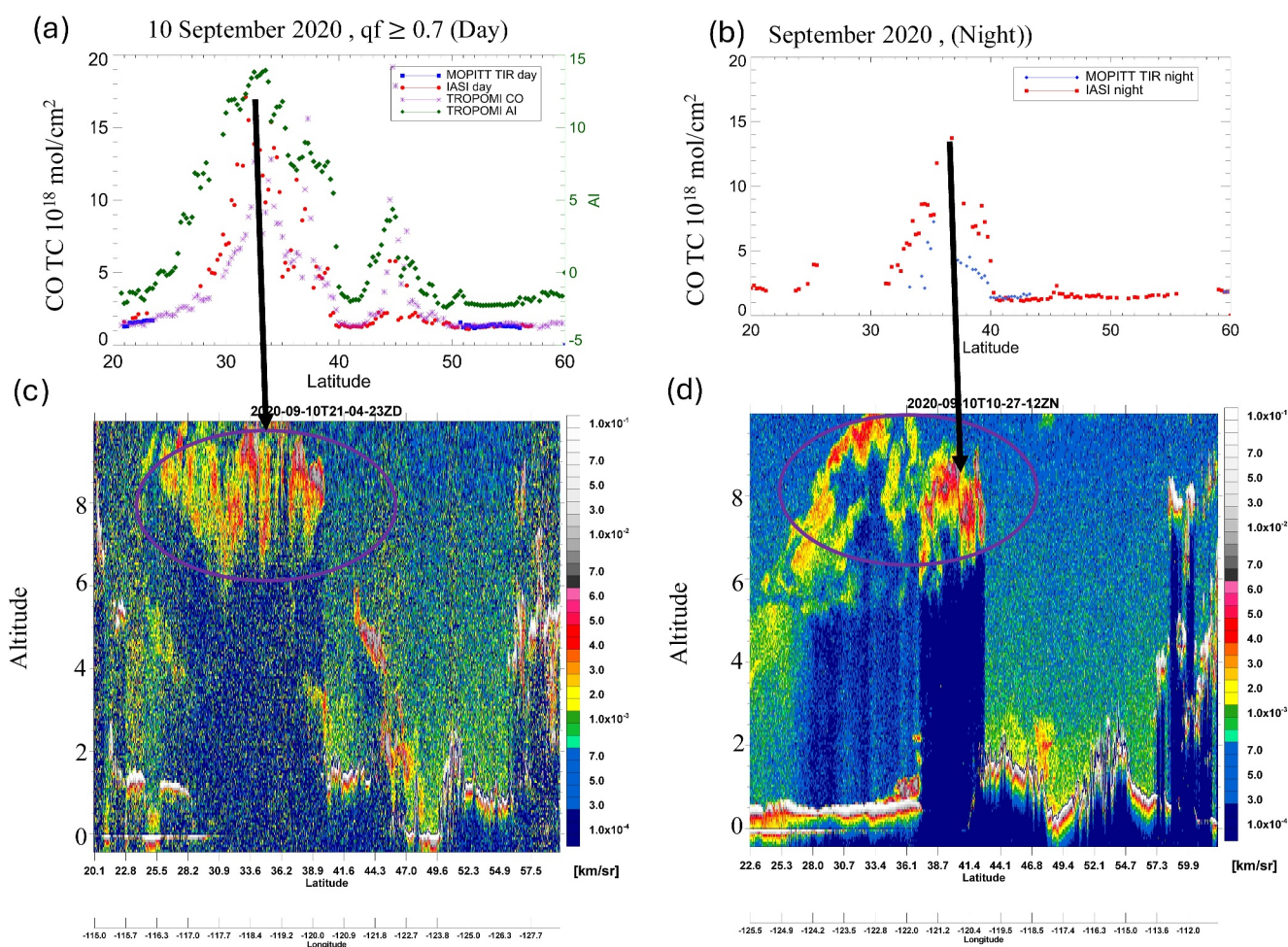


**Figure 7.** (a, b) Tropospheric Monitoring Instrument (TROPOMI), Infrared Atmospheric Sounding Interferometer (IASI), and Measurements of Pollution in the Troposphere (MOPITT) CO TC, (c, d) CALIPSO for day and night, respectively on 10 September 2020. The MOPITT, IASI, and TROPOMI data are typically averaged over longitude widths along the CALIPSO path. The unit “km/sr” stands for “kilometers per steradian.”

(FLEXPART) dispersion model and accounting for TROPOMI’s vertical sensitivity as reflected by the AVKs, the average bias between TROPOMI and aircraft remote sensing measurements was reduced to +10%. Rowe et al. (2022) highlighted the intricate relationship between aerosols and trace gases and stressed the importance of careful interpretation of satellite data, particularly in wildfire-affected regions.

Repeating the previous analysis using the clear TROPOMI CO retrieval ( $qf = 1$ ) shown in Figure 8 leads to the removal of most of the CO data along the CALIPSO daytime track (cyan) compared to Figure 6a ( $qf \geq 0.7$  (cloudy)). This suggests that the high CO values are linked to the presence of thick aerosol layers, which are sometimes misinterpreted as cloudy conditions, as indicated by Figure 8b.

### 3.4. The Impact of Aerosols

The analysis in Section 3.1, along with the case study in Section 3.3, indicates that during periods of elevated aerosol loading within dense smoke plumes during the 2020 Western U.S. wildfire season, TROPOMI retrievals showed significantly higher CO values compared to MOPITT. Similarly, IASI recorded higher CO TC values during these events than the corresponding MOPITT measurements. These discrepancies are attributed to larger CO concentrations near the surface, as reflected in the CO profiles from each instrument.

To explore the aerosol loading issue, we selected contrasting cases in which the aerosol load is low, but the CO TC levels are relatively high, above  $3 \times 10^{18}$  molecules/cm<sup>2</sup>. Three regions were chosen for this contrasting analysis: the Amazon, southern Africa, and central Asia. Figure 9a–9c display the spatial distribution of the gridded



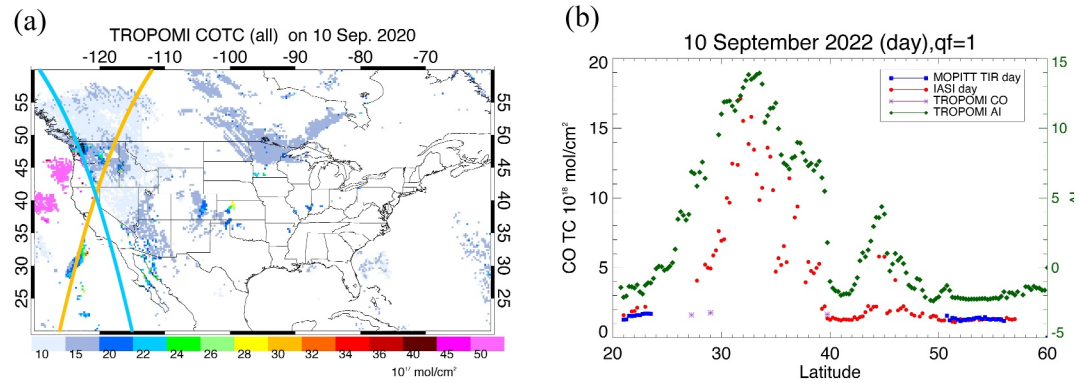


**Figure 8.** (a) TROPOMI CO TC (non-located) over North America and (b) Tropospheric Monitoring Instrument (TROPOMI), Infrared Atmospheric Sounding Interferometer, and MOPITT CO TC data along CALIPSO track on 10 September 2020 for the case with  $qf = 1$  for the TROPOMI retrievals.

( $0.25^\circ \times 0.25^\circ$ ) collocated CO TC data averaged for September, derived from TROPOMI (with  $qf = 0.7, 1$ , low clouds), IASI, and MOPITT data, respectively, over the Amazon region. The corresponding figures for southern Africa and central Asia are shown in Figs 2s–5s in Supporting Information S1. CO total columns from the three data sets display a similar spatial pattern. In general, the Amazon region experiences high biomass fire activity during the dry season, between June and November. The fire activity begins in June and peaks in September. The enhanced CO columns shown in Figure 9 are mainly influenced by extreme wildfire emissions that occurred in September 2020, when about 40,000 km<sup>2</sup> were burned because of a severe drought in the region (Pugh et al., 2022).

The daily CO TC values derived from the three sensors along with the TROPOMI AI, averaged over the Amazon region for September, are presented in Figure 10. Figure 10a shows the non-located CO data (all the data), while Figure 10b shows the collocated data. The daily TROPOMI AI is low although the measurements were made during the time of a pollution event driven by biomass burning. Unlike the PNW fires, where the AI values exceeded 8 (Figures 3d and 7), the AI values over the Amazon region did not exceed 0.5. In Figure 10, all sensors exhibit a generally similar temporal pattern, with a peak occurring in the middle of the month. However, IASI's peak values are more prominent and tend to be higher compared to those from MOPITT and TROPOMI, especially between September 15th and twentieth. While MOPITT and TROPOMI show a generally consistent pattern, MOPITT's data fluctuates, whereas TROPOMI's data is smoother, as shown in Figure 10a (non-located). This difference can be attributed to the lower MOPITT sampling frequency relative to TROPOMI, resulting from its lower temporal resolution (3 days). Consequently, in the collocated data sets, this agreement is more pronounced, although IASI's peaks are still higher (Figure 10b).

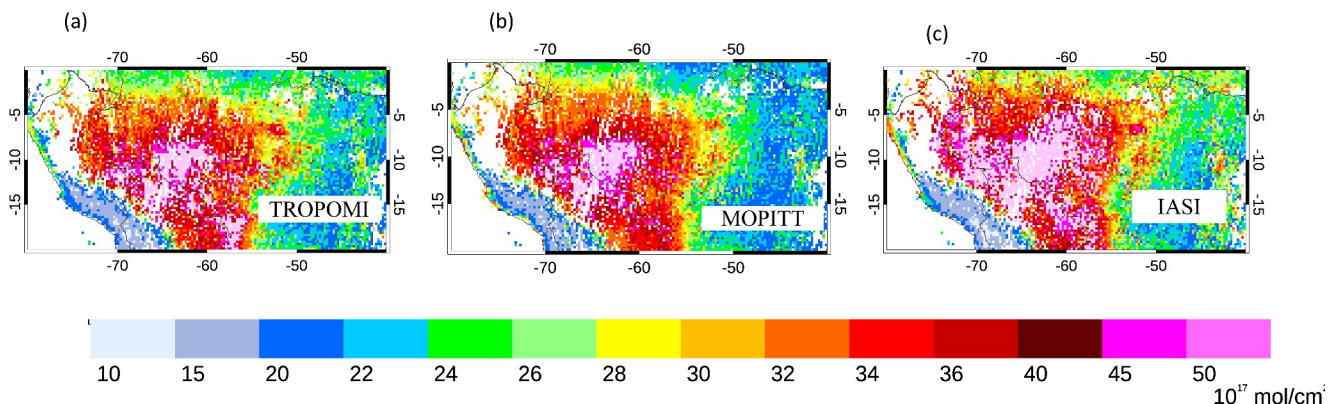


**Figure 9.** Spatial variations of collocated CO Total Column over the Amazon region of TROPOMI data with  $qf > 0.7$  (a), MOPITT Joint (b), and IASI (c), for September 2020. The data were gridded on a  $0.25^\circ \times 0.25^\circ$  grid.

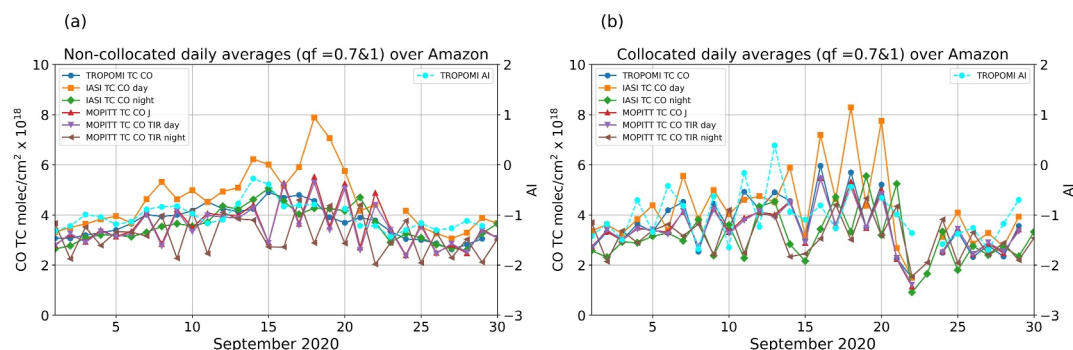


**Figure 10.** Daily time series of MOPITT, IASI and TROPOMI data, averaged over Amazon region, in September 2020 of non-collocated data (a) and collocated data (b). TROPOMI AI is indicated by the cyan dashed line, with the AI values shown in the right y-axis.

Since the magnitude of the aerosol AI signal depends mainly on AOD, aerosol height, and aerosol absorption, Amazon biomass burning aerosols possibly are mixed with sulfate aerosols (Patra et al., 2005) (non-absorbing) at lower altitudes (Torres et al., 2013). Also, this highlights the different transport mechanisms of fire emissions over the PNW and the Amazon region. Torres et al. (2020) examined the TROPOMI AOD and AI over many fire-prone regions and found that the very high AI values are associated with pyroCb events such as the Australian smoke plume on 2 January 2020. In contrast, they found that the monthly average values of TROPOMI AI over South America during the September 2019 fires did not exceed 1.5, which is consistent with the current results. Unfortunately, CALIPSO profiles are not available for the same region and time to validate the aerosol height. Accordingly, there is better agreement among the three sensors when the AI values are low (Figures 9 and 10), while the discrepancies increase at very high AI values (Figures 3d and 7), as observed in the PNW analysis. This agreement is more pronounced between TROPOMI and MOPITT CO TC, whereas IASI still shows some higher values, particularly during the period of September 15–20.

The same analysis was repeated over southern Africa (Figures 2s and 3s) and central Asia (Figures 4s and 5s) during September 2020 and both regions demonstrated good general consistency, especially between TROPOMI and MOPITT CO TC data, where the AI values were small, less than one. Regarding IASI's discrepancies on some days, this can be attributed to the greater variability in the lower and middle troposphere layers, along with the correlation between layers, allowing information from the middle tropospheric layer to be projected to the lower troposphere layer (George et al., 2015; Lutsch et al., 2022).

Specific fire types, such as pyroCb may lead to differences in the vertical distribution of CO over the affected areas, impacting the sensitivity of each instrument to detect and measure CO concentrations. This is evidenced by the observed variation in offset between TROPOMI and MOPITT/IASI, highlighting the importance of considering the influence of different fire types and aerosol distributions when interpreting satellite-based CO measurements. This might explain the varying offset between TROPOMI and MOPITT/IASI CO values across different AI levels and the association of high AI conditions with pyroCb fire types.

#### 4. Summary and Conclusions

In September 2020, the western United States experienced unprecedented severe wildfires relative to the recent fire record in terms of human impact, burn severity, and size. The major difference between the 2020 fires and previous fires was the occurrence of extreme regional scale drying and rapid strong winds blowing from the west that simultaneously occurred with multiple ignitions (Reilly et al., 2022). Strong westerly winds that developed during the 2020 fires and were notable for their intensity and timing and contributed to the spread and severity of the wildfires. These westerly winds likely played a significant role in driving the rapid expansion of the fires across the affected regions (Reilly et al., 2022). The CO emissions of the western U.S. 2020 wildfire season were more than three times the 2001–2019 averaged emissions (Albores et al., 2023).

This study investigated the comparability of CO retrievals from MOPITT, IASI, and TROPOMI, particularly under wildfire conditions, to understand the factors influencing discrepancies between the sensor measurements. In general, all the instruments show excellent agreement under typical atmospheric CO conditions (column

abundances less than  $3 \times 10^{18}$  molecules/cm<sup>2</sup>). Strong enhancements in the CO TCs were clearly observed by all sensors over the western United States, and parts of the eastern U.S. because of atmospheric transport of the fire emissions. However, notable discrepancies were observed in the CO data from the three sensors, particularly in regions with elevated CO TC values. IASI and TROPOMI consistently showed higher CO values over the western U.S. region compared to MOPITT. These discrepancies highlighted the importance of the differences in sampling, vertical sensitivity, and retrieval algorithms of the three sensors. Rowe et al. (2022) demonstrated that biases observed in TROPOMI data compared to aircraft remote sensing measurements may be attributed to the influence of aerosols on the retrieval of CO. They suggested that TROPOMI CO signals can be enhanced under high aerosol load conditions due to multiple scattering.

Analysis of MOPITT TIR and IASI daily CO profiles over the NA domain in September 2020 revealed that the IASI retrievals suggested higher CO abundances near the surface than the MOPITT TIR retrievals during the fire episodes. The high IASI CO values near the surface are probably the result of the differences in the covariance matrices used in the IASI and MOPITT retrievals. Relative to MOPITT, the IASI covariance matrix provides a loose constraint on the retrievals near the surface, which could lead to high surface concentrations due to correlations in the retrievals between the surface and the middle troposphere, especially during episodic fire events (George et al., 2015; Lutsch et al., 2022). The extremely high IASI and TROPOMI CO observations over the PNW coincide with the high TROPOMI AI values. High positive AI values typically indicate the presence of absorbing aerosols. Analysis of CALIPSO data suggested that these high TROPOMI AI values were associated with dense (absorbing) smoke aerosols at high altitudes (~8 km) which coincided with the period of exceptionally high CO observations by IASI and TROPOMI instruments over the PNW. One possible explanation is that high AI conditions are associated with specific fire types, such as pyroCb, leading to differences in the vertical distribution of CO over these fires and affecting the sensitivity of each instrument. Other regions, such as the Amazon, with relatively low aerosol loading but high CO TC levels (above  $3 \times 10^{18}$  molecules/cm<sup>2</sup>), were chosen to explore the aerosol impact on the CO columns. Unlike the PNW where the AI values exceeded 8, the averaged AI over the other regions did not exceed 0. The analysis here demonstrated better agreement between TROPOMI and MOPITT CO TC when the AI values are low, whereas discrepancies between the two sensors increase at high AI values, as was shown in the case of the PNW analysis. Under extreme conditions of high aerosol loading within thick smoke plumes, the TROPOMI CO retrievals exhibited high values relative to the corresponding MOPITT retrievals. The current analysis highlights the potential challenges with TROPOMI's retrieval under high AI conditions. These challenges may be attributed to the association of high AI conditions with specific fire types, such as pyrocumulonimbus (pyroCb) events. PyroCb events can lead to differences in the vertical distribution of CO over affected areas, which in turn impacts the sensitivity of each instrument in detecting and measuring CO concentrations.

Given the correlation between TROPOMI high CO levels and AI values, it is important to independently validate the use of AI data for quality filtering to ensure reliability and accuracy. This validation process may include comparing AI data with measurements from aircraft or ground-based instruments. Additionally, modeling techniques can be employed to optimize the utilization of AI data by simulating various scenarios and evaluating their impact on data quality.

While this study offers insights into the differences in the CO distribution from the three satellite instruments, further investigations using model-based analyses are recommended to address existing gaps. Integrating satellite data with atmospheric models can provide a deeper understanding of the underlying processes driving CO variations and refine interpretations. Expanding the scope of this study to include other regions and a longer time period would also be valuable. By examining CO distributions over diverse geographical areas and over an extended timeframe, we can better understand the factors contributing to discrepancies, reliability, and limitations of satellite-based CO retrievals.

### Data Availability Statement

MOPITT data were obtained from the NASA Earthdata website (<https://search.earthdata.nasa.gov/search?q=carbon%20monoxide&fi=MOPITT>, last access: 30 March 2024). TROPOMI data were obtained from the NASA Earthdata website (<https://search.earthdata.nasa.gov/search?q=carbon%20monoxide&fi=TROPOMI>, last access: 3 April 2024). IASI data were obtained through the AERIS website (<https://iasi.aeris-data.fr/co/>, last access: 3 April 2024).

access: 9 May 2024). CALIPSO data were obtained ([https://asdc.larc.nasa.gov/data/CALIPSO/LID\\_L1-Standard-V4-11/2020/09/](https://asdc.larc.nasa.gov/data/CALIPSO/LID_L1-Standard-V4-11/2020/09/)), last access: 1 June 2024).

### Acknowledgments

The authors would like to thank the Canadian Space Agency (CSA) for their financial support of this research. NCAR (National Center for Atmospheric Research) is sponsored by the National Science Foundation and operated by the University Corporation for Atmospheric Research. The NCAR MOPITT project is supported by the National Aeronautics and Space Administration (NASA) EOS Program. The MOPITT team acknowledges support from the CSA. The authors acknowledge the AC SAF project, EUMETSAT and the AERIS infrastructure for generating and distributing the IASI CO data. We acknowledge TROPOMI science teams for making TROPOMI Level 2 data publicly available. Sentinel-5 Precursor is part of the EU Copernicus program, and Copernicus Sentinel data have been used.

### References

- Abatzoglou, J. T., Rupp, D. E., O'Neill, L. W., & Sadeq, M. (2021). Compound extremes drive the western Oregon wildfires of September 2020. *Geophysical Research Letters*, 48(8), e2021GL092520. <https://doi.org/10.1029/2021gl092520>
- Albores, I. S., Buchholz, R. R., Ortega, I., Emmons, L. K., Hannigan, J. W., Lacey, F., et al. (2023). Continental-scale atmospheric impacts of the 2020 western US wildfires. *Atmospheric Environment*, 294, 119436. <https://doi.org/10.1016/j.atmosenv.2022.119436>
- Andreae, M. O., & Merlet, P. (2001). Emission of trace gases and aerosols from biomass burning. *Global Biogeochemical Cycles*, 15(4), 955–966. <https://doi.org/10.1029/2000gb001382>
- Apituley, A., Pedergrana, M., Sneep, M., Pepijn Veeffkind, J., Loyola, D., Landgraf, J., & Borsdorff, T. (2020). Sentinel-5 precursor/TROPOMI level 2 product user manual carbon monoxide [Dataset]. *Royal Netherlands Meteorological Institute (KNMI)*. <https://sentinel.esa.int/documents/247904/2474726/Sentinel-5P-Level-2-Product-User-Manual-Carbon-Monoxide.pdf>
- Astoreca, R., Hurtmans, D., Coheur, P., Hadji-Lazaro, J., George, M., Safieddine, S., & Clerbaux, C. (2021). PRODUCT USER MANUAL near real-time partial and total IASI CO Metop-C [Dataset]. [https://acsaf.org/docs/pum/Product\\_User\\_Manual\\_IASI-C\\_CO\\_Nov\\_2021.pdf](https://acsaf.org/docs/pum/Product_User_Manual_IASI-C_CO_Nov_2021.pdf)
- Barret, B., Gouzenes, Y., Le Flochmoen, E., & Ferrant, S. (2021). Retrieval of Metop-A/IASI N<sub>2</sub>O profiles and validation with NDACC FTIR data. *Atmosphere*, 12(2), 219. <https://doi.org/10.3390/atmos12020219>
- Barret, B., Le Flochmoen, E., Sauvage, B., Pavelin, E., Matricardi, M., & Cammas, J. P. (2011). The detection of post-monsoon tropospheric ozone variability over south Asia using IASI data. *Atmospheric Chemistry and Physics*, 11(18), 9533–9548. <https://doi.org/10.5194/acp-11-9533-2011>
- Barret, B., Loicq, P., Le Flochmoen, E., Bennouna, Y., Hadji-Lazaro, J., Hurtmans, D., & Sauvage, B. (2024). Validation of 12 years (2008–2019) of IASI-CO with IAGOS aircraft observations. *EGU sphere*, 2024, 1–29.
- Bates, T. S., Kelly, K. C., Johnson, J. E., & Gammon, R. H. (1995). Regional and seasonal variations in the flux of oceanic carbon monoxide to the atmosphere. *Journal of Geophysical Research*, 100(D11), 23093–23101. <https://doi.org/10.1029/95jd02737>
- Borsdorff, T., Campos, T., Kille, N., Volkamer, R., & Landgraf, J. (2022). Vertical information of CO from TROPOMI total column measurements in context of the CAMS-IFS data assimilation scheme. *Atmospheric Measurement Techniques Discussions*, 1–20.
- Borsdorff, T., Hasekamp, O. P., Wassmann, A., & Landgraf, J. (2014). Insights into tikhonov regularization: Application to trace gas column retrieval and the efficient calculation of total column averaging kernels. *Atmospheric Measurement Techniques*, 7(2), 523–535. <https://doi.org/10.5194/amt-7-523-2014>
- Borsdorff, T., Hu, H., Hasekamp, O., Sussmann, R., Rettinger, M., Hase, F., et al. (2018). Mapping carbon monoxide pollution from space down to city scales with daily global coverage. *Atmospheric Measurement Techniques*, 11(10), 5507–5518. <https://doi.org/10.5194/amt-11-5507-2018>
- Borsdorff, T., Hu, H., Nédélec, P., Aben, I., & Landgraf, J. (2017). Carbon monoxide column retrieval for clear-sky and cloudy atmospheres: A full-mission data set from SCIAMACHY 2.3 μm reflectance measurements. *Atmospheric Measurement Techniques*, 10(5), 1769–1782. <https://doi.org/10.5194/amt-10-1769-2017>
- Boynard, A., Hurtmans, D., Koukouli, M. E., Goutail, F., Bureau, J., Safieddine, S., et al. (2016). Seven years of IASI ozone retrievals from FORLI: Validation with independent total column and vertical profile measurements. *Atmospheric Measurement Techniques*, 9(9), 4327–4353. <https://doi.org/10.5194/amt-9-4327-2016>
- Buchholz, R. R., Park, M., Worden, H. M., Tang, W., Edwards, D. P., Gaubert, B., et al. (2022). New seasonal pattern of pollution emerges from changing North American wildfires. *Nature Communications*, 13(1), 1–9. <https://doi.org/10.1038/s41467-022-29623-8>
- Busa, E., Gugamsetty, B., Kalluri, R. O. R., Kotalo, R. G., Tandule, C. R., Thotli, L. R., & Palle, S. N. R. (2022). Diurnal, seasonal, and vertical distribution of carbon monoxide levels and their potential sources over a semi-arid region, India. *Atmosfera*, 35(1), 165–178. <https://doi.org/10.20937/atm.52808>
- Clerbaux, C., Boynard, A., Clarisse, L., George, M., Hadji-Lazaro, J., Herbin, H., et al. (2009). Monitoring of atmospheric composition using the thermal infrared IASI/MetOp sounder. *Atmospheric Chemistry and Physics*, 9(16), 6041–6054. <https://doi.org/10.5194/acp-9-6041-2009>
- Deeter, M., Francis, G., Gille, J., Mao, D., Martínez-Alonso, S., Worden, H., et al. (2022). The MOPITT version 9 CO product: Sampling enhancements and validation [Dataset]. *Atmospheric Measurement Techniques*, 15(8), 2325–2344. <https://doi.org/10.5194/amt-15-2325-2022>
- Deeter, M. N., Edwards, D. P., Francis, G. L., Gille, J. C., Mao, D., Martínez-Alonso, S., et al. (2019). Radiance-based retrieval bias mitigation for the MOPITT instrument: The version 8 product. *Atmospheric Measurement Techniques*, 12(8), 4561–4580. <https://doi.org/10.5194/amt-12-4561-2019>
- Deeter, M. N., Edwards, D. P., Francis, G. L., Gille, J. C., Martínez-Alonso, S., Worden, H. M., & Sweeney, C. (2017). A climate-scale satellite record for carbon monoxide: The MOPITT version 7 product. *Atmospheric Measurement Techniques*, 10(7), 2533–2555. <https://doi.org/10.5194/amt-10-2533-2017>
- Deeter, M. N., Edwards, D. P., Gille, J. C., & Drummond, J. R. (2007). Sensitivity of MOPITT observations to carbon monoxide in the lower troposphere. *Journal of Geophysical Research*, 112(D24). <https://doi.org/10.1029/2007jd008929>
- Deeter, M. N., Edwards, D. P., Gille, J. C., Emmons, L. K., Francis, G., Ho, S. P., et al. (2010). The MOPITT version 4 CO product: Algorithm enhancements, validation, and long-term stability. *Journal of Geophysical Research*, 115(D7). <https://doi.org/10.1029/2009jd013005>
- Deeter, M. N., Emmons, L. K., Francis, G. L., Edwards, D. P., Gille, J. C., Warner, J. X., et al. (2003). Operational carbon monoxide retrieval algorithm and selected results for the MOPITT instrument. *Journal of Geophysical Research*, 108(D14). <https://doi.org/10.1029/2002jd003186>
- Deeter, M. N., Mao, D., Martínez-Alonso, S., Worden, H. M., Andreae, M. O., & Schlager, H. (2021). Impacts of MOPITT cloud detection revisions on observation frequency and mapping of highly polluted scenes. *Remote Sensing of Environment*, 262, 112516. <https://doi.org/10.1016/j.rse.2021.112516>
- Deeter, M. N., Martínez-Alonso, S., Edwards, D. P., Emmons, L. K., Gille, J. C., Worden, H. M., et al. (2013). Validation of MOPITT Version 5 thermal-infrared, near-infrared, and multispectral carbon monoxide profile retrievals for 2000–2011. *Journal of Geophysical Research: Atmospheres*, 118(12), 6710–6725. <https://doi.org/10.1002/jgrd.50272>
- Deeter, M. N., Martínez-Alonso, S., Edwards, D. P., Emmons, L. K., Gille, J. C., Worden, H. M., et al. (2014). The MOPITT version 6 product: Algorithm enhancements and validation. *Atmospheric Measurement Techniques*, 7(11), 3623–3632. <https://doi.org/10.5194/amt-7-3623-2014>
- Deeter, M. N., Worden, H. M., Edwards, D. P., Gille, J. C., & Andrews, A. E. (2012). Evaluation of MOPITT retrievals of lower-tropospheric carbon monoxide over the United States. *Journal of Geophysical Research*, 117(D13). <https://doi.org/10.1029/2012jd017553>
- Deeter, M. N., Worden, H. M., Gille, J. C., Edwards, D. P., Mao, D., & Drummond, J. R. (2011). MOPITT multispectral CO retrievals: Origins and effects of geophysical radiance errors. *Journal of Geophysical Research*, 116(D15), D15303. <https://doi.org/10.1029/2011jd015703>

- DellaSala, D. A., Bond, M. L., Hanson, C. T., Hutto, R. L., & Odion, D. C. (2014). Complex early seral forests of the Sierra Nevada: What are they and how can they be managed for ecological integrity? *Natural Areas Journal*, *34*(3), 310–324. <https://doi.org/10.3375/043.034.0317>
- Dillon, G. K., Holden, Z. A., Morgan, P., Crimmins, M. A., Heyerdahl, E. K., & Luce, C. H. (2011). Both topography and climate affected forest and woodland burn severity in two regions of the western US, 1984 to 2006. *Ecosphere*, *2*(12), 1–33. <https://doi.org/10.1890/es11-00271.1>
- Drummond, J. R., Zanjani, Z. V., Nichitui, F., & Zou, J. (2022). A 20-year review of the performance and operation of the MOPITT instrument. *Advances in Space Research*, *70*(10), 3078–3091. <https://doi.org/10.1016/j.asr.2022.09.010>
- Emmons, L., Deeter, M., Edwards, D., Gille, J., Ziskin, D., Attié, J. L., et al. (2002). Validation of MOPITT retrievals of carbon monoxide. In *IEEE international geoscience and remote sensing symposium* (Vol. 6, pp. 3174–3176). IEEE. <https://doi.org/10.1109/igars.2002.1027121>
- Emmons, L. K., Deeter, M. N., Gille, J. C., Edwards, D. P., Attié, J. L., Warner, J., et al. (2004). Validation of Measurements of Pollution in the Troposphere (MOPITT) CO retrievals with aircraft in situ profiles. *Journal of Geophysical Research*, *109*(D3). <https://doi.org/10.1029/2003jd004101>
- Evers, C., Holz, A., Busby, S., & Nielsen-Pincus, M. (2022). Extreme winds alter influence of fuels and topography on megafire burn severity in seasonal temperate rainforests under record fuel aridity. *Fire*, *5*(2), 41. <https://doi.org/10.3390/fire5020041>
- Finlay, S. E., Moffat, A., Gazzard, R., Baker, D., & Murray, V. (2012). Health impacts of wildfires. *PLoS currents*, *4*. <https://doi.org/10.1371/4f959951cce2c>
- George, M., Clerbaux, C., Bouarar, I., Coheur, P. F., Deeter, M. N., Edwards, D. P., et al. (2015). An examination of the long-term CO records from MOPITT and IASI: Comparison of retrieval methodology. *Atmospheric Measurement Techniques*, *8*(10), 4313–4328. <https://doi.org/10.5194/amt-8-4313-2015>
- George, M., Clerbaux, C., Hurtmans, D., Turquety, S., Coheur, P. F., Pommier, M., et al. (2009). Carbon monoxide distributions from the IASI/METOP mission: Evaluation with other space-borne remote sensors. *Atmospheric Chemistry and Physics*, *9*(21), 8317–8330. <https://doi.org/10.5194/acp-9-8317-2009>
- Higuera, P. E., & Abatzoglou, J. T. (2021). Record-setting climate enabled the extraordinary 2020 fire season in the western United States. *Global Change Biology*, *27*(1), 1–2. <https://doi.org/10.1111/gcb.15388>
- Juliano, T. W., Jiménez, P. A., Kosović, B., Eidhammer, T., Thompson, G., Berg, L. K., et al. (2022). Smoke from 2020 United States wildfires responsible for substantial solar energy forecast errors. *Environmental Research Letters*, *17*(3), 034010. <https://doi.org/10.1088/1748-9326/ac5143>
- Kerzenmacher, T., Dils, B., Kumps, N., Blumenstock, T., Clerbaux, C., Coheur, P. F., et al. (2012). Validation of IASI FORLI carbon monoxide retrievals using FTIR data from NDACC. *Atmospheric Measurement Techniques*, *5*(11), 2751–2761. <https://doi.org/10.5194/amt-5-2751-2012>
- Kim, M. H., Omar, A. H., Tackett, J. L., Vaughan, M. A., Winker, D. M., Trepte, C. R., et al. (2018). The CALIPSO version 4 automated aerosol classification and Lidar ratio selection algorithm. *Atmospheric Measurement Techniques*, *11*(11), 6107–6135. <https://doi.org/10.5194/amt-11-6107-2018>
- Kittaka, C., Winker, D. M., Vaughan, M. A., Omar, A., & Remer, L. A. (2011). Intercomparison of column aerosol optical depths from CALIPSO and MODIS-Aqua. *Atmospheric Measurement Techniques*, *4*(2), 131–141. <https://doi.org/10.5194/amt-4-131-2011>
- Klonecki, A., Pommier, M., Clerbaux, C., Ancellet, G., Cammas, J. P., Coheur, P. F., et al. (2012). Assimilation of IASI satellite CO fields into a global chemistry transport model for validation against aircraft measurements. *Atmospheric Chemistry and Physics*, *12*(10), 4493–4512. <https://doi.org/10.5194/acp-12-4493-2012>
- Krol, M. S. B. M. A. P. W. F. P., Houweling, S., Bregman, B., Van den Broek, M., Segers, A., Van Velthoven, P., et al. (2005). The two-way nested global chemistry-transport zoom model TM5: Algorithm and applications. *Atmospheric Chemistry and Physics*, *5*(2), 417–432. <https://doi.org/10.5194/acp-5-417-2005>
- Lamarque, J. F., Edwards, D. P., Emmons, L. K., Gille, J. C., Wilhelm, O., Gerbig, C., et al. (2003). Identification of CO plumes from MOPITT data: Application to the August 2000 Idaho-Montana forest fires. *Geophysic*.
- Landgraf, J., Scheepmaker, R., Borsdorff, T., Hu, H., Houweling, S., Butz, A., et al. (2016). Carbon monoxide total column retrievals from TROPOMI shortwave infrared measurements. *Atmospheric Measurement Techniques*, *9*(10), 4955–4975. <https://doi.org/10.5194/amt-9-4955-2016>
- Lapina, K., Honrath, R. E., Owen, R. C., Val Martin, M., & Pfister, G. (2006). Evidence of significant large-scale impacts of boreal fires on ozone levels in the midlatitude Northern Hemisphere free troposphere. *Geophysical Research Letters*, *33*(10). <https://doi.org/10.1029/2006gl025878>
- Liu, J., Bowman, K. W., Schimel, D. S., Parazoo, N. C., Jiang, Z., Lee, M., et al. (2017). Contrasting carbon cycle responses of the tropical continents to the 2015–2016 El Niño. *Science*, *358*(6360), eaam5690. <https://doi.org/10.1126/science.aam5690>
- Lutsch, E., Wunch, D., Jones, D. B., Clerbaux, C., Hannigan, J. W., He, T. L., & Worden, H. M. (2022). Can the data assimilation of CO from MOPITT or IASI constrain high-latitude wildfire emissions? A case study of the 2017 Canadian wildfires. *Authorea Preprints*.
- Marey, H. S., Drummond, J. R., Jones, D., Worden, H., Deeter, M. N., Gille, J., & Mao, D. (2022). Analysis of improvements in MOPITT observational coverage over Canada. *Atmospheric Measurement Techniques*, *15*(3), 701–719. <https://doi.org/10.5194/amt-15-701-2022>
- Mass, C. F., Ovens, D., Conrick, R., & Saltenberger, J. (2021). The September 2020 wildfires over the Pacific Northwest. *Weather and Forecasting*, *36*(5), 1843–1865. <https://doi.org/10.1175/waf-d-21-0028.1>
- McClure, C. D., & Jaffe, D. A. (2018). US particulate matter air quality improves except in wildfire-prone areas. *Proceedings of the National Academy of Sciences* (Vol. 115(31), 7901–7906). <https://doi.org/10.1073/pnas.1804353115>
- Nakata, M., Sano, I., Mukai, S., & Kokhanovsky, A. (2022). Characterization of wildfire smoke over complex terrain using satellite observations, ground-based observations, and meteorological models. *Remote Sensing*, *14*(10), 2344. <https://doi.org/10.3390/rs14102344>
- Pandey, P. C. (2022). Highlighting the role of earth observation Sentinel5P TROPOMI in monitoring volcanic eruptions: A report on hunga Tonga, a submarine volcano. *Remote Sensing Letters*, *13*(9), 912–923. <https://doi.org/10.1080/2150704x.2022.2106799>
- Parrish, D. D., Singh, H. B., Molina, L., & Madronich, S. (2011). Air quality progress in North American megacities: A review. *Atmospheric Environment*, *45*(39), 7015–7025. <https://doi.org/10.1016/j.atmosenv.2011.09.039>
- Patra, P. K., Behera, S. K., Herman, J. R., Maksyutov, S., Akimoto, H., & Yamagata, Y. (2005). The Indian summer monsoon rainfall: Interplay of coupled dynamics, radiation and cloud microphysics. *Atmospheric Chemistry and Physics*, *5*(8), 2181–2188. <https://doi.org/10.5194/acp-5-2181-2005>
- Phuleria, H., Ducret-Stich, R., Ineichen, A., Tsai, M., & Liu, L. J. (2011). Trace metal composition of ambient PM<sub>2.5</sub> and PM<sub>10</sub> and their spatiotemporal variation near a major highway in an alpine valley in Switzerland. *Epidemiology*, *22*(1), S288–S289. <https://doi.org/10.1097/01.ede.0000392586.47768.d4>
- Pommier, M., Law, K. S., Clerbaux, C., Turquety, S., Hurtmans, D., Hadji-Lazaro, J., et al. (2010). IASI carbon monoxide validation over the Arctic during POLARCAT spring and summer campaigns. *Atmospheric Chemistry and Physics*, *10*(21), 10655–10678. <https://doi.org/10.5194/acp-10-10655-2010>

- Pugh, B. E., Colley, M., Dugdale, S. J., Edwards, P., Flitcroft, R., Holz, A., et al. (2022). A possible role for river restoration enhancing biodiversity through interaction with wildfire. *Global Ecology and Biogeography*, *31*(10), 1990–2004. <https://doi.org/10.1111/geb.13555>
- Reilly, M. J., Zuspan, A., Halofsky, J. S., Raymond, C., McEvoy, A., Dye, A. W., et al. (2022). Cascadia Burning: The historic, but not historically unprecedented, 2020 wildfires in the Pacific Northwest, USA. *Ecosphere*, *13*(6), e4070. <https://doi.org/10.1002/ecs2.4070>
- Robbins, D., Poulsen, C., Siems, S., & Proud, S. (2022). Improving discrimination between clouds and optically thick aerosol plumes in geostationary satellite data. *Atmospheric Measurement Techniques*, *15*(9), 3031–3051. <https://doi.org/10.5194/amt-15-3031-2022>
- Rodgers, C. D. (2000). Inverse methods for atmospheric sounding: Theory and practice, *Series on Atmospheric, Oceanic Planetary Physics* (Vol. 2). World Scientific.
- Rowe, J. P., Zarzana, K. J., Kille, N., Borsdorff, T., Goudar, M., Lee, C. F., et al. (2022). Carbon monoxide in optically thick wildfire smoke: Evaluating TROPOMI using CU airborne SOF column observations. *ACS Earth and Space Chemistry*, *6*(7), 1799–1812. <https://doi.org/10.1021/acsearthspacechem.2c00048>
- Russell, E. N., Loikith, P. C., Ajibade, I., Done, J. M., & Lower, C. (2024). The meteorology and impacts of the September 2020 Western United States extreme weather event. *Weather and Climate Extremes*, *43*, 100647. <https://doi.org/10.1016/j.wace.2024.100647>
- Schneising, O., Buchwitz, M., Reuter, M., Bovensmann, H., & Burrows, J. P. (2020). Severe Californian wildfires in November 2018 observed from space: The carbon monoxide perspective. *Atmospheric Chemistry and Physics*, *20*(6), 3317–3332. <https://doi.org/10.5194/acp-20-3317-2020>
- Scholze, M., Knorr, W., Arnell, N. W., & Prentice, I. C. (2006). A climate-change risk analysis for world ecosystems. *Proceedings of the National Academy of Sciences* (Vol. 103(35)), 13116–13120. <https://doi.org/10.1073/pnas.0601816103>
- Torres, O., Ahn, C., & Chen, Z. (2013). Improvements to the OMI near UV aerosol algorithm using A-train CALIOP and AIRS observations. *Atmospheric Measurement Techniques Discussions*, *6*(3), 5621–5652. <https://doi.org/10.5194/amt-6-3257-2013>
- Torres, O., Jethva, H., Ahn, C., Jaross, G., & Loyola, D. G. (2020). TROPOMI aerosol products: Evaluation and observations of synoptic-scale carbonaceous aerosol plumes during 2018–2020. *Atmospheric Measurement Techniques*, *13*(12), 6789–6806. <https://doi.org/10.5194/amt-13-6789-2020>
- Turquet, S., Hurtmans, D., Hadji-Lazaro, J., Coheur, P. F., Clerbaux, C., Josset, D., & Tsamalis, C. (2009). Tracking the emission and transport of pollution from wildfires using the IASI CO retrievals: Analysis of the summer 2007 Greek fires. *Atmospheric Chemistry and Physics*, *9*(14), 4897–4913. <https://doi.org/10.5194/acp-9-4897-2009>
- Varga, K., Jones, C., Trugman, A., Carvalho, L. M., McLoughlin, N., Seto, D., & Daum, K. (2022). Megafires in a warming world: What wildfire risk factors led to California's largest recorded wildfire. *Fire*, *5*(1), 16. <https://doi.org/10.3390/fire5010016>
- Vaughan, M. A., Young, S. A., Winker, D. M., Powell, K. A., Omar, A. H., Liu, Z., & Hostetler, C. A. (2004). Fully automated analysis of space-based lidar data: An overview of the CALIPSO retrieval algorithms and data products. *Laser radar techniques for atmospheric sensing*, 5575, 16–30.
- Veefkind, J. P., Aben, I., McMullan, K., Förster, H., De Vries, J., Otter, G., et al. (2012). TROPOMI on the ESA sentinel-5 precursor: A GMES mission for global observations of the atmospheric composition for climate, air quality and ozone layer applications. *Remote Sensing of Environment*, *120*, 70–83. <https://doi.org/10.1016/j.rse.2011.09.027>
- Voulgarakis, A., Marlier, M. E., Faluvegi, G., Shindell, D. T., Tsigaridis, K., & Mangeon, S. (2015). Interannual variability of tropospheric trace gases and aerosols: The role of biomass burning emissions. *Journal of Geophysical Research: Atmospheres*, *120*(14), 7157–7173. <https://doi.org/10.1002/2014jd022926>
- Westerling, A. L. (2016). Increasing western US forest wildfire activity: Sensitivity to changes in the timing of spring. *Philosophical Transactions of the Royal Society B: Biological Sciences*, *371*(1696), 20150178. <https://doi.org/10.1098/rstb.2015.0178>
- Wilmot, T. Y., Mallia, D. V., Hallar, A. G., & Lin, J. C. (2022). Wildfire plumes in the Western US are reaching greater heights and injecting more aerosols aloft as Winker activity intensifies. *Scientific Reports*, *12*(1), 12400. <https://doi.org/10.1038/s41598-022-16607-3>
- Winker, D. M., Hunt, W. H., & McGill, M. J. (2007). Initial performance assessment of CALIOP. *Geophysical Research Letters*, *34*(19). <https://doi.org/10.1029/2007gl030135>
- Winker, D. M., Vaughan, M. A., Omar, A., Hu, Y., Powell, K. A., Liu, Z., & Young, S. A. (2009). Overview of the CALIPSO mission and CALIOP data processing algorithms. *Journal of Atmospheric and Oceanic Technology*, *26*(11), 2310–2323. <https://doi.org/10.1175/2009jtecha1281.1>
- Worden, H. M., Deeter, M. N., Edwards, D. P., Gille, J. C., Drummond, J. R., & Nédélec, P. (2010). Observations of near-surface carbon monoxide from space using MOPITT multispectral retrievals. *Journal of Geophysical Research*, *115*(D18). <https://doi.org/10.1029/2010jd014242>
- Worden, J., Jiang, Z., Jones, D. B., Alvarado, M., Bowman, K., Frankenberg, C., et al. (2013). El Niño, the 2006 Indonesian peat fires, and the distribution of atmospheric methane. *Geophysical Research Letters*, *40*(18), 4938–4943. <https://doi.org/10.1002/grl.50937>
- Xie, Y., Lin, M., Decharme, B., Delire, C., Horowitz, L. W., Lawrence, D. M., et al. (2022). Tripling of western US particulate pollution from wildfires in a warming climate. *Proceedings of the National Academy of Sciences* (Vol. 119(14)), e2111372119. <https://doi.org/10.1073/pnas.2111372119>
- Yin, Y., Ciaï, P., Chevallier, F., Van der Werf, G. R., Fanin, T., Broquet, G., et al. (2016). Variability of fire carbon emissions in equatorial Asia and its nonlinear sensitivity to El Niño. *Geophysical Research Letters*, *43*(19), 10–472. <https://doi.org/10.1002/2016gl070971>
- Youssef, H., Liouise, C., Roblou, L., Assamoi, E. M., Salonen, R. O., Maesano, C., & Annesi-Maesano, I. (2014). Quantifying wildfires exposure for investigating health-related effects. *Atmospheric Environment*, *97*, 239–251. <https://doi.org/10.1016/j.atmosenv.2014.07.041>